

Large-Scale Low-Rank Matrix Learning with Nonconvex Regularizers

Quanming Yao, *Member IEEE*, James T. Kwok, *Fellow IEEE*, Taifeng Wang, *Member IEEE*,
and Tie-Yan Liu, *Fellow IEEE*

Abstract—Low-rank modeling has many important applications in computer vision and machine learning. While the matrix rank is often approximated by the convex nuclear norm, the use of nonconvex low-rank regularizers has demonstrated better empirical performance. However, the resulting optimization problem is much more challenging. Recent state-of-the-art requires an expensive full SVD in each iteration. In this paper, we show that for many commonly-used nonconvex low-rank regularizers, the singular values obtained from the proximal operator can be automatically threshold. This allows the proximal operator to be efficiently approximated by the power method. We then develop a fast proximal algorithm and its accelerated variant with inexact proximal step. A convergence rate of $O(1/T)$, where T is the number of iterations, can be guaranteed. Furthermore, we show the proposed algorithm can be parallelized, and the resultant algorithm achieves nearly linear speedup w.r.t. the number of threads. Extensive experiments are performed on matrix completion and robust principal component analysis. Significant speedup over the state-of-the-art is observed.

Index Terms—Low-rank matrix learning, Nonconvex regularization, Proximal algorithm, Parallel algorithm, Matrix completion, Robust principle component analysis

1 INTRODUCTION

LOW-rank matrix learning is a central issue in many machine learning and computer vision problems. For example, matrix completion [1], which is one of the most successful approaches in collaborative filtering, assumes that the target rating matrix is low-rank. Besides collaborative filtering, matrix completion has also been used on tasks such as video and image processing [2], [3], [4], [5], [6]. Another important use of low-rank matrix learning is robust principal component analysis (RPCA) [7], which assumes that the target matrix is low-rank and also corrupted by sparse noise. RPCA has been popularly used in computer vision applications such as shadow removal, background modeling [7], [8], [9], and robust photometric stereo [10]. Besides, low-rank matrix learning has also been used in face recognition [11] and subspace clustering [12].

However, minimization of the matrix rank is NP-hard [1]. To alleviate this problem, a common approach is to use a convex surrogate such as the nuclear norm (which is the sum of singular values of the matrix). It is known that the nuclear norm is the tightest convex lower bound of the rank. Though the nuclear norm is non-smooth, the resultant optimization problem can be solved efficiently using modern tools such as the proximal algorithm [13], [14], [15], Frank-Wolfe algorithm [16], and active subspace selection method [17].

Despite the success of the nuclear norm, recently there have been numerous attempts to use nonconvex surrogates that better approximate the rank function. The key idea is

that the larger, and thus more informative, singular values should be less penalized. Example nonconvex low-rank regularizers include the capped- ℓ_1 penalty [18], log-sum penalty (LSP) [19], truncated nuclear norm (TNN) [3], [9], smoothly clipped absolute deviation (SCAD) [20], and min-max concave penalty (MCP) [21]. They have been applied on various computer vision tasks, such as image denoising [6] and background modeling [9]. Empirically, these nonconvex regularizers achieve better recovery performance than the convex nuclear norm regularizer. Recently, theoretical results have also been established [22].

However, the resultant nonconvex optimization problem is much more challenging. Most existing optimization algorithms that work with the nuclear norm cannot be applied. A general approach that can still be used is the concave-convex procedure [23], which decomposes the nonconvex regularizer into a difference of convex functions [3], [18]. However, a sequence of relaxed optimization problems have to be solved, and can be computationally expensive [24], [25]. A more efficient approach is the recently proposed iteratively re-weighted nuclear norm (IRNN) algorithm [5]. It is based on the observation that existing nonconvex regularizers are concave with non-increasing super-gradients. Each IRNN iteration only involves computing the super-gradient of the regularizer and a singular value decomposition (SVD). However, performing SVD on a $m \times n$ matrix takes $O(mn^2)$ time (assuming $m \geq n$), and can be expensive on large matrices.

Recently, the proximal algorithm has been used for nonconvex low-rank matrix learning [3], [5], [9], [26]. However, it requires the full SVD to solve the proximal operator, which can be expensive. In this paper, we observe that for the commonly-used nonconvex low-rank regularizers [3], [9], [18], [19], [20], [21], the singular values obtained from the corresponding proximal operator can be automatically

- Q. Yao and J. Kwok are with the Department of Computer Science and Engineering, Hong Kong University of Science and Technology, Clear Water Bay, Hong Kong. E-mails: {qyaoaa, jamesk}@cse.ust.hk
- T. Wang and T. Liu are with Microsoft Research Asia, Beijing, China 100010. E-mails: {taifengw, tyliu}@microsoft.com

thresholded. One then only needs to find the leading singular values/vectors in order to generate the next iterate. Moreover, instead of computing the proximal operator on a large matrix, one only needs to use the matrix projected onto its leading subspace. The matrix size is significantly reduced and the proximal operator can be made much more efficient. Besides, by using the power method [27], a good approximation of this subspace can be efficiently obtained.

While the proposed procedure can be readily used with the standard proximal algorithm, its convergence properties are not directly applicable as the proximal step here is only approximately solved. In the sequel, we will show that inexactness on the proximal step can be controlled, and a $O(1/T)$ convergence rate can still be guaranteed. Moreover, the algorithm can be further speeded up using acceleration. Effectiveness of the proposed algorithms is demonstrated on two popular low-rank matrix learning applications, namely matrix completion and robust principal component analysis (RPCA). For matrix completion, we show that additional speedup is possible by exploring the problem's "sparse plus low-rank" structure; whereas for RPCA, we extend the proposed algorithm so that it can handle the two parameter blocks involved in the RPCA formulation.

With the popularity of multicore shared-memory platforms, we parallelize the proposed algorithms so as to handle much larger data sets. We will show that they can achieve almost linear speedup w.r.t. the number of threads.

Experiments are performed on both synthetic and real-world data sets. Results show that the proposed nonconvex low-rank matrix learning algorithms can be several orders faster than the state-of-the-art, and outperform other approaches including factorization and the use of nuclear norm regularization.

Preliminary results of this paper have been reported in [28]. In this full version, we speed up the algorithm with acceleration, and demonstrate how it can be applied to two important instances of low-rank matrix learning problems, namely matrix completion and RPCA. Besides, we show how the proposed algorithms can be parallelized. More extensive empirical evaluations are also performed on both the sequential and parallel versions of the algorithms.

Notation: In the sequel, vectors are denoted by lowercase boldface, matrices by uppercase boldface, and the transpose by the superscript $(\cdot)^\top$. For a square matrix \mathbf{X} , $\text{tr}(\mathbf{X})$ is its trace. For a rectangle matrix \mathbf{X} , $\|\mathbf{X}\|_F = \sqrt{\text{tr}(\mathbf{X}^\top \mathbf{X})}$ is its Frobenius norm, and $\|\mathbf{X}\|_* = \sum_i \sigma_i(\mathbf{X})$, where $\sigma_i(\mathbf{X})$ is the i th leading singular value of \mathbf{X} , is the nuclear norm. Given $\mathbf{x} = [x_i] \in \mathbb{R}^m$, $\text{Diag}(\mathbf{x})$ constructs a $m \times m$ diagonal matrix whose i th diagonal element is x_i . \mathbf{I} denotes the identity matrix. For a differentiable function f , we use ∇f for its gradient. For a nonsmooth function, we use ∂f for its subdifferential, i.e., $\partial f(\mathbf{x}) = \{\mathbf{s} : f(\mathbf{y}) \geq f(\mathbf{x}) + \mathbf{s}^\top(\mathbf{y} - \mathbf{x})\}$.

2 BACKGROUND

2.1 Proximal Algorithm

In this paper, we consider low-rank matrix learning problems of the form

$$\min_{\mathbf{X}} F(\mathbf{X}) \equiv f(\mathbf{X}) + \lambda r(\mathbf{X}), \quad (1)$$

where f is a smooth loss, r is a nonsmooth low-rank regularizer, and λ is a regularization parameter. We make the following assumptions on f .

- A1. f is not necessarily convex, but is differentiable with ρ -Lipschitz continuous gradient, i.e., $\|\nabla f(\mathbf{X}_1) - \nabla f(\mathbf{X}_2)\|_F \leq \rho \|\mathbf{X}_1 - \mathbf{X}_2\|_F$. Without loss of generality, we assume that $\rho \leq 1$.
- A2. f is bounded below, i.e., $\inf f(\mathbf{X}) > -\infty$, and $\lim_{\|\mathbf{X}\|_F \rightarrow \infty} f(\mathbf{X}) = \infty$.

In recent years, the proximal algorithm [29] has been popularly used for solving (1). At iteration t , it produces

$$\mathbf{X}_{t+1} = \text{prox}_{\frac{\lambda}{\tau} r}(\mathbf{X}_t - \frac{1}{\tau} \nabla f(\mathbf{X}_t)), \quad (2)$$

where $\tau > \rho$ is the stepsize, and

$$\text{prox}_{\frac{\lambda}{\tau} r}(\mathbf{Z}) \equiv \arg \min_{\mathbf{X}} \frac{1}{2} \|\mathbf{X} - \mathbf{Z}\|_F^2 + \lambda r(\mathbf{X}) \quad (3)$$

is the proximal operator [29]. The proximal step in (2) can also be rewritten as $\mathbf{X}_{t+1} = \arg \min_{\mathbf{Y}} \text{tr}(\nabla f(\mathbf{X}_t)^\top (\mathbf{Y} - \mathbf{X}_t)) + \frac{\tau}{2} \|\mathbf{Y} - \mathbf{X}_t\|_F^2 + \lambda r(\mathbf{Y})$.

When f and r are convex, the proximal algorithm converges to the optimal solution at a rate of $O(1/T)$, where T is the number of iterations. This can be further accelerated to the rate of $O(1/T^2)$, by replacing \mathbf{X}_t in (2) with a proper linear combination of \mathbf{X}_t and \mathbf{X}_{t-1} [30]. Recently, the accelerated proximal algorithm has been extended to problems where f or r may be nonconvex [25], [31]. The state-of-the-art is the nonmonotone accelerated proximal gradient (nmAPG) algorithm [25] (Algorithm 1). Each iteration may perform two proximal steps (steps 4 and 8). Acceleration is performed in step 3. The objective is then checked to determine whether \mathbf{X}_{t+1}^a is accepted (step 5). As the problem is nonconvex, its convergence rate is still open. However, empirically it is much faster.

Algorithm 1 Nonmonotone APG (nmAPG) [25].

Input: choose $\tau > \rho$, $\delta > 0$ and $\eta \in [0, 1]$;
1: initialize $\mathbf{X}_0 = \mathbf{X}_1 = \mathbf{X}_1^a = 0$, $\alpha_0 = \alpha_1 = 1$, $b_1 = F(\mathbf{X}_1)$ and $q_1 = 1$;
2: **for** $t = 1, 2, \dots, T$ **do**
3: $\mathbf{Y}_t = \mathbf{X}_t + \frac{\alpha_{t-1}}{\alpha_t}(\mathbf{X}_t^a - \mathbf{X}_{t-1}) + \frac{\alpha_{t-1}-1}{\alpha_t}(\mathbf{X}_t - \mathbf{X}_{t-1})$;
4: $\mathbf{X}_{t+1}^a = \text{prox}_{\frac{\lambda}{\tau} r}(\mathbf{Y}_t - \frac{1}{\tau} \nabla f(\mathbf{Y}_t))$;
5: **if** $F(\mathbf{X}_{t+1}^a) \leq b_t - \frac{\delta}{2} \|\mathbf{X}_{t+1}^a - \mathbf{Y}_t\|_F^2$ **then**
6: $\mathbf{X}_{t+1} = \mathbf{X}_{t+1}^a$;
7: **else**
8: $\mathbf{X}_{t+1}^p = \text{prox}_{\frac{\lambda}{\tau} r}(\mathbf{X}_t - \frac{1}{\tau} \nabla f(\mathbf{X}_t))$;
9: $\mathbf{X}_{t+1} = \begin{cases} \mathbf{X}_{t+1}^a & \text{if } F(\mathbf{X}_{t+1}^a) \leq F(\mathbf{X}_{t+1}^p); \\ \mathbf{X}_{t+1}^p & \text{otherwise} \end{cases}$;
10: **end if**
11: $\alpha_{t+1} = \frac{1}{2}(\sqrt{4\alpha_t^2 + 1} + 1)$;
12: $b_{t+1} = \frac{1}{q_{t+1}}(\eta q_t b_t + F(\mathbf{X}_{t+1}))$ where $q_{t+1} = \eta q_t + 1$;
13: **end for**
14: **return** \mathbf{X}_{T+1} .

2.2 Nonconvex Low-Rank Regularizers

For the proximal algorithm to be successful, the proximal operator has to be efficient. The following shows that the

proximal operator of the nuclear norm $\|\cdot\|_*$ has a closed-form solution.

Proposition 2.1 ([32]). $\text{prox}_{\mu\|\cdot\|_*}(\mathbf{X}) = \mathbf{U}(\mathbf{\Sigma} - \mu\mathbf{I})_+ \mathbf{V}^\top$, where $\mathbf{U}\mathbf{\Sigma}\mathbf{V}^\top$ is the SVD of \mathbf{X} , and $(\mathbf{A})_+ = [\max(A_{ij}, 0)]$.

While the (convex) nuclear norm makes low-rank optimization easier, it may not be a good enough approximation of the matrix rank [3], [5], [6], [9], [26]. As mentioned in Section 1, a number of nonconvex surrogates have been recently proposed. In this paper, we make the following assumption on the low-rank regularizer r in (1), which is satisfied by all nonconvex low-rank regularizers in Table 1.

- A3. r is possibly non-smooth and nonconvex, and of the form $r(\mathbf{X}) = \sum_{i=1}^m \hat{r}(\sigma_i(\mathbf{X}))$, where $\hat{r}(\alpha)$ is concave and non-decreasing for $\alpha \geq 0$ and $\hat{r}(0) = 0$.

TABLE 1

\hat{r} 's for some popular nonconvex low-rank regularizers. For the TNN regularizer, $\theta \in \{1, \dots, n\}$ is the number of leading singular values that are not penalized; for SCAD, $\theta > 2$; and for the others, $\theta > 0$.

	$\mu\hat{r}(\sigma_i(\mathbf{X}))$
capped- ℓ_1 [18]	$\mu \min(\sigma_i(\mathbf{X}), \theta)$
LSP [19]	$\mu \log(\frac{1}{\theta}\sigma_i(\mathbf{X}) + 1)$
TNN [3], [9]	$\begin{cases} \mu\sigma_i(\mathbf{X}) & \text{if } i > \theta \\ 0 & \text{otherwise} \end{cases}$
SCAD [20]	$\begin{cases} \mu\sigma_i(\mathbf{X}) & \text{if } \sigma_i(\mathbf{X}) \leq \mu \\ \frac{-\sigma_i^2(\mathbf{X}) + 2\theta\mu\sigma_i(\mathbf{X}) - \mu^2}{2(\theta-1)} & \text{if } \mu < \sigma_i(\mathbf{X}) \leq \theta\mu \\ \frac{(\theta+1)\mu^2}{2} & \text{otherwise} \end{cases}$
MCP [21]	$\begin{cases} \mu\sigma_i(\mathbf{X}) - \frac{\sigma_i^2(\mathbf{X})}{2\theta} & \text{if } \sigma_i(\mathbf{X}) \leq \theta\mu \\ \frac{\theta\mu^2}{2} & \text{otherwise} \end{cases}$

Recently, the iteratively reweighted nuclear norm (IRNN) algorithm [5] has been proposed to handle this nonconvex low-rank matrix optimization problem. In each iteration, it solves a subproblem in which the original nonconvex regularizer is approximated by a weighted version of the nuclear norm $\|\mathbf{X}\|_{\mathbf{w}} = \sum_{i=1}^m w_i \sigma_i(\mathbf{X})$ and $0 \leq w_1 \leq \dots \leq w_m$. The subproblem has a closed-form solution, but SVD is needed which takes $O(mn^2)$ time. Other solvers that are designed for specific nonconvex low-rank regularizers include [8] (for capped- ℓ_1), [3], [9] (for TNN), and [21] (for MCP). All these (including IRNN) perform SVD in each iteration, which takes $O(mn^2)$ time and are slow.

While the proximal algorithm has mostly been used on convex problems, recently it is also applied to nonconvex problems [3], [5], [6], [8], [9], [26]. The generalized proximal gradient (GPG) algorithm [26] is the first proximal algorithm which can handle all the above nonconvex regularizers. In particular, its proximal operator can be computed as follows.

Proposition 2.2 (Generalized singular value thresholding (GSVT) [26]). For any r satisfying assumption A3, $\text{prox}_{\mu r}(\mathbf{Z}) = \mathbf{U}\text{Diag}(\mathbf{y}^*)\mathbf{V}^\top$, where $\mathbf{U}\mathbf{\Sigma}\mathbf{V}^\top$ is the SVD of \mathbf{Z} , and $\mathbf{y}^* = [y_i^*]$ with

$$y_i^* \in \arg \min_{y_i \geq 0} \frac{1}{2} (y_i - \sigma_i(\mathbf{Z}))^2 + \mu\hat{r}(y_i). \quad (4)$$

In [26], problem (4) is solved by fixed-point iteration. However, closed-form solutions indeed exist for regularizers in Table 1 [24]. Nevertheless, Proposition 2.2 still involves SVD, which takes $O(mn^2)$ time.

3 PROPOSED ALGORITHM

In this section, we show how the proximal algorithm can be made much faster by using approximate GSVT.

3.1 Automatic Thresholding of Singular Values

The following Proposition shows that y_i^* in (4) becomes zero when $\sigma_i(\mathbf{Z})$ is smaller than a regularizer-specific threshold. Proof can be found in Appendix C.1.

Proposition 3.1. There exists a threshold $\gamma > 0$ such that $y_i^* = 0$ when $\sigma_i(\mathbf{Z}) \leq \gamma$.

Together with Proposition 2.2, solving the proximal operator (3) only needs the leading singular values/vectors of \mathbf{Z} . For the nonconvex regularizers in Table 1, simple closed-form solutions of γ can be obtained by examining the optimality conditions of (4). Proof can be found in Appendix C.2.

Corollary 3.2. The γ values for the following regularizers are:

- Capped- ℓ_1 : $\gamma = \min(\sqrt{2\theta\mu}, \mu)$;
- LSP: $\gamma = \min(\frac{\mu}{\theta}, \theta)$;
- TNN: $\gamma = \max(\mu, \sigma_{\theta+1}(\mathbf{Z}))$;
- SCAD: $\gamma = \mu$;
- MCP: $\gamma = \sqrt{\theta\mu}$ if $0 < \theta < 1$, and μ otherwise.

This can also be used with the nuclear norm. It can be shown that $\gamma = \frac{\lambda}{\tau}$, and $y_i^* = \max(\sigma_i(\mathbf{A}) - \frac{\lambda}{\tau}, 0)$. However, since our focus is on nonconvex regularizers, the case for nuclear norm will not be further pursued in the sequel.

3.2 Approximate GSVT

Proposition 2.2 computes the proximal operator by exact SVD. In this section, we show that one can use approximate SVD, which is more efficient.

3.2.1 Reducing the Size of SVD

Assume that \mathbf{Z} has \hat{k} singular values larger than γ , then we only need to a rank- k SVD on \mathbf{Z} with $k \geq \hat{k}$. Let the rank- \hat{k} SVD of \mathbf{Z} be $\mathbf{U}_{\hat{k}}\mathbf{\Sigma}_{\hat{k}}\mathbf{V}_{\hat{k}}^\top$. The following Proposition shows that $\text{prox}_{\mu r}(\mathbf{Z})$ can be obtained from the proximal operator on a smaller matrix.¹ The proof can be found in Appendix C.3.

Proposition 3.3. Assume that $\mathbf{Q} \in \mathbb{R}^{m \times k}$, where $k \geq \hat{k}$, is orthogonal and $\text{span}(\mathbf{U}_{\hat{k}}) \subseteq \text{span}(\mathbf{Q})$. Then, $\text{prox}_{\mu r}(\mathbf{Z}) = \mathbf{Q}\text{prox}_{\mu r}(\mathbf{Q}^\top \mathbf{Z})$.

3.2.2 Obtaining an Approximate GSVT

To obtain such a \mathbf{Q} , we use the power method [27] (Algorithm 2) which has been recently used to approximate the SVT in nuclear norm minimization [15], [17]. As in [17], we set the number of power iterations to 3. Warm-start can be used via matrix \mathbf{R} in Algorithm 2. This is particularly useful because of the iterative nature of proximal algorithm. Obtaining an approximate \mathbf{Q} using Algorithm 2 takes $O(mnk)$ time. As in [14], [34], [35], the PROPACK

1. We noticed a similar result in [33] after the conference version of this paper [28] has been accepted. However, [33] only considers the case where r is the nuclear norm regularizer.

algorithm [36] can also be used to obtain \mathbf{Q} in $O(mnk)$ time. However, it finds the \mathbf{Q} exactly and cannot benefit from warm-start. Hence, though it has the same time complexity as power method, empirically it is much less efficient [15].

Algorithm 2 Powermethod(\mathbf{Z}, \mathbf{R}).

Input: $\mathbf{Z} \in \mathbb{R}^{m \times n}$, $\mathbf{R} \in \mathbb{R}^{n \times k}$ and the number of power iterations $J = 3$.

- 1: $\mathbf{Y}_1 = \mathbf{Z}\mathbf{R}$;
- 2: **for** $j = 1, 2, \dots, J$ **do**
- 3: $\mathbf{Q}_j = \text{QR}(\mathbf{Y}_j)$; // QR decomposition (returning only the \mathbf{Q} matrix)
- 4: $\mathbf{Y}_{j+1} = \mathbf{Z}(\mathbf{Z}^\top \mathbf{Q}_j)$;
- 5: **end for**
- 6: **return** \mathbf{Q}_J .

The approximate GSVT procedure is shown in Algorithm 3. Step 1 uses the power method to efficiently obtain an orthogonal matrix \mathbf{Q} that approximates $\text{span}(\mathbf{U}_{\hat{k}})$. Step 2 performs a small SVD. Though this SVD is still exact, $\mathbf{Q}^\top \mathbf{Z}$ is much smaller than \mathbf{Z} ($k \times n$ vs $m \times n$), and $\text{SVD}(\mathbf{Q}^\top \mathbf{Z})$ takes only $O(nk^2)$ time. In step 3, the singular values Σ_{ii} 's are thresholded using Corollary 3.2. Steps 6-8 obtains an (approximate) $\text{prox}_{\mu r}(\mathbf{Z})$ using Proposition 2.2. The time complexity for GSVT is reduced from $O(mn^2)$ to $O(mnk)$.

Algorithm 3 Approximate GSVT: ApproxGSVT($\mathbf{Z}, \mathbf{R}, \mu$).

Input: $\mathbf{Z} \in \mathbb{R}^{m \times n}$ and $\mathbf{R} \in \mathbb{R}^{n \times k}$ for warm-start;

- 1: $\mathbf{Q} = \text{PowerMethod}(\mathbf{Z}, \mathbf{R})$;
- 2: $[\mathbf{U}, \Sigma, \mathbf{V}] = \text{SVD}(\mathbf{Q}^\top \mathbf{Z})$;
- 3: $a = \text{number of } \Sigma_{ii} \text{'s that are } > \gamma \text{ in Corollary 3.2}$;
- 4: $\mathbf{U}_a = a \text{ leading columns of } \mathbf{U}$;
- 5: $\mathbf{V}_a = a \text{ leading columns of } \mathbf{V}$;
- 6: **for** $i = 1, 2, \dots, a$ **do**
- 7: obtain y_i^* from (4);
- 8: **end for**
- 9: **return** low-rank components of $\tilde{\mathbf{X}}$ ($\mathbf{Q}\mathbf{U}_a$, $\text{Diag}([y_1^*, \dots, y_a^*])$ and \mathbf{V}_a^\top), and \mathbf{V} .

3.3 Inexact Proximal Step

In this section, the proximal step will be inexact, and so it can utilize the approximate GSVT in Algorithm 3. Inexact proximal step has been considered in [37], [38]. However, r in (1) is assumed to be convex in [38]. Attouch et al. [37] considered nonconvex r , but they require a difficult and expensive condition to control inexactness (an example is provided in Appendix B).

Let $\mathbf{A} = \mathbf{X} - \frac{1}{\tau} \nabla f(\mathbf{X})$. The following shows that the objective F is always decreased (as $\tau > \rho$) after an exact proximal step.

Lemma 3.4 ([24], [37]). $F(\text{prox}_{\frac{\lambda}{\tau} r}(\mathbf{A})) \leq F(\mathbf{X}) - \frac{\tau - \rho}{2} \|\text{prox}_{\frac{\lambda}{\tau} r}(\mathbf{A}) - \mathbf{X}\|_F^2$.

Motivated by this Lemma, we propose to control the proximal step's inexactness by Algorithm 4 (note that $\mathbf{X} =$

\mathbf{X}_t for the proximal gradient algorithm in (2)). An approximate proximal step solution $\tilde{\mathbf{X}}_p$ is generated in step 4, and we try to ensure

$$F(\tilde{\mathbf{X}}_p) \leq F(\mathbf{X}) - c_1 \|\tilde{\mathbf{X}}_p - \mathbf{X}\|_F^2, \quad (5)$$

where $c_1 = \frac{\tau - \rho}{4}$ (note that this is less stringent than the condition in Lemma 3.4). If (5) holds, we accept $\tilde{\mathbf{X}}_p$; otherwise, we improve $\tilde{\mathbf{X}}_p$ by using $\tilde{\mathbf{V}}_{p-1}$ to warm-start the next iterate. The following Proposition shows convergence of Algorithm 4. The proof can be found in Appendix C.4.

Proposition 3.5. If $k \geq \hat{k}_{\mathbf{A}}$, where $\hat{k}_{\mathbf{A}}$ is the number of singular values in \mathbf{A} larger than γ , then $\lim_{p \rightarrow \infty} \tilde{\mathbf{X}}_p = \text{prox}_{\frac{\lambda}{\tau} r}(\mathbf{A})$.

Algorithm 4 Inexact proximal step: InexactPS(\mathbf{X}, \mathbf{R}).

Input: $\mathbf{X} \in \mathbb{R}^{m \times n}$, and $\mathbf{R} \in \mathbb{R}^{n \times k}$ for warm-start;

- 1: $\mathbf{A} = \mathbf{X} - \frac{1}{\tau} \nabla f(\mathbf{X})$;
- 2: $\tilde{\mathbf{V}}_0 = \mathbf{R}$;
- 3: **for** $p = 1, 2, \dots$ **do**
- 4: $[\tilde{\mathbf{X}}_p, \tilde{\mathbf{V}}_p] = \text{ApproxGSVT}(\mathbf{A}, \tilde{\mathbf{V}}_{p-1}, \frac{\lambda}{\tau})$;
- 5: **if** $F(\tilde{\mathbf{X}}_p) \leq F(\mathbf{X}) - c_1 \|\tilde{\mathbf{X}}_p - \mathbf{X}\|_F^2$ **then**
- 6: **break**;
- 7: **end if**
- 8: **end for**
- 9: **return** $\tilde{\mathbf{X}}_p$.

3.4 The Complete Procedure

The complete procedure for solving (1) is shown in Algorithm 5, and will be called FaNCL (Fast NonConvex Lowrank). Similar to [15], [17], we perform warm-start using the column spaces of the previous iterates (\mathbf{V}_t and \mathbf{V}_{t-1}). For further speedup, we employ a continuation strategy at step 3 as in [5], [14], [34]. Specifically, λ_t is initialized to a large value and then decreases gradually.

Algorithm 5 FaNCL (Fast NonConvex Low-rank) algorithm.

Input: choose $\tau > \rho$, $\lambda_0 > \lambda$ and $\nu \in (0, 1)$;

- 1: initialize $\mathbf{V}_0, \mathbf{V}_1 \in \mathbb{R}^n$ as random Gaussian matrices and $\mathbf{X}_1 = 0$;
- 2: **for** $t = 1, 2, \dots, T$ **do**
- 3: $\lambda_t = (\lambda_{t-1} - \lambda)\nu^t + \lambda$;
- 4: $\mathbf{R}_t = \text{QR}([\mathbf{V}_t, \mathbf{V}_{t-1}])$; // warm start
- 5: $\mathbf{X}_{t+1} = \text{InexactPS}(\mathbf{X}_t, \mathbf{R}_t)$;
- 6: **end for**
- 7: **return** \mathbf{X}_{T+1} .

Assume that evaluations of f and ∇f take $O(mn)$ time, which is valid for many applications such as matrix completion and RPCA. Let r_t be the rank of \mathbf{X}_t at the t th iteration, and $k_t = r_t + r_{t-1}$. In Algorithm 5, step 4 takes $O(nk_t^2)$ time; and step 5 takes $O(mnpk_t)$ time as \mathbf{R}_t has k_t columns. The iteration time complexity is thus $O(mnpk_t)$. In the experiment, we set $p = 1$, which is enough to guarantee (5) empirically. The iteration time complexity of Algorithm 5 thus reduces to $O(mnk_t)$. In contrast, exact GSVT takes $O(mn^2)$ time, and is much slower as $k_t \ll n$. Besides, the space complexity of Algorithm 5 is $O(mn)$.

3.5 Convergence Analysis

The inexact proximal algorithm is first considered in [38], which assumes r to be convex. The nonconvex extension is considered in [37]. However, as discussed in Section 3.3, they use an expensive condition to control inexactness of the proximal step. Thus, their analysis cannot be applied here.

It is known that \hat{r} in Assumption A3 can be decomposed as a difference of convex functions [24]. The following Proposition shows that r also admits such a decomposition. The proof is in Appendix C.5.

Proposition 3.6. r can be decomposed as $\check{r} - \tilde{r}$, where \check{r} and \tilde{r} are convex.

Based on this decomposition, we introduce the definition of critical point.

Definition 1 ([39]). If $\mathbf{0} \in \nabla f(\mathbf{X}) + \lambda(\partial\check{r}(\mathbf{X}) - \partial\tilde{r}(\mathbf{X}))$, then \mathbf{X} is a critical point of F .

The following Proposition shows that Algorithm 5 generates a bounded sequence. The proof is in Appendix C.6.

Proposition 3.7. The sequence $\{\mathbf{X}_t\}$ generated from Algorithm 5 is bounded, and has at least one limit point.

Let $\mathcal{G}_{\frac{\lambda}{\tau}r}(\mathbf{X}_t) = \mathbf{X}_t - \text{prox}_{\frac{\lambda}{\tau}r}(\mathbf{X}_t - \frac{1}{\tau}\nabla f(\mathbf{X}_t))$, which is known as the proximal mapping of F at \mathbf{X}_t [29]. If $\mathcal{G}_{\frac{\lambda}{\tau}r}(\mathbf{X}_t) = \mathbf{0}$, \mathbf{X}_t is a critical point of (1) [24], [37]. This motivates the use of $\|\mathcal{G}_{\frac{\lambda}{\tau}r}(\mathbf{X}_t)\|_2^2$ to measure convergence in [31]. However, $\|\mathcal{G}_{\frac{\lambda}{\tau}r}(\mathbf{X}_t)\|_2^2$ cannot be used here as r is nonconvex and the proximal step is inexact. As Proposition 3.7 guarantees the existence of limit points, we use $\|\mathbf{X}_{t+1} - \mathbf{X}_t\|_F^2$ instead to measure convergence. If the proximal step is exact, $\|\mathcal{G}_{\frac{\lambda}{\tau}r}(\mathbf{X}_t)\|_F^2 = \|\mathbf{X}_{t+1} - \mathbf{X}_t\|_F^2$. The following Corollary shows convergence of Algorithm 5. Its proof can be found in Appendix C.7.

Corollary 3.8. $\min_{t=1,\dots,T} \|\mathbf{X}_{t+1} - \mathbf{X}_t\|_F^2 \leq \frac{F(\mathbf{X}_1) - \inf F}{c_1 T}$.

The following Theorem shows that any limit point is also a critical point. The proof is in Appendix C.8.

Theorem 3.9. Assume that Algorithm 4 returns \mathbf{X} only when $\mathbf{X} = \text{prox}_{\frac{\lambda}{\tau}r}(\mathbf{X} - \frac{1}{\tau}\nabla f(\mathbf{X}))$ (i.e., the input is returned as output only if it is a limit point). Let $\{\mathbf{X}_{t_j}\}$ be a subsequence of $\{\mathbf{X}_t\}$ generated by Algorithm 5 such that $\lim_{t_j \rightarrow \infty} \mathbf{X}_{t_j} = \mathbf{X}_*$. Then, \mathbf{X}_* is a critical point of (1).

3.6 Acceleration

In convex optimization, acceleration has been commonly used to speed up convergence of proximal algorithms [30]. Recently, it has also been extended to nonconvex optimization [25], [31]. A state-of-the-art algorithm is the nmAPG [25] (Algorithm 1).

In this section, we integrate nmAPG with FaNCL. The whole procedure is shown in Algorithm 6. The accelerated iterate is obtained in step 4. If the resultant inexact proximal step solution can achieve a sufficient decrease (step 7) as in (5), this iterate is accepted (step 8); otherwise, we choose the inexact proximal step solution obtained with the non-accelerated iterate \mathbf{X}_t (step 10). Note that step 10 is the same as step 5 of Algorithm 5. Thus, the iteration time complexity of Algorithm 6 is at most twice that of Algorithm 5, and still

$O(mnk_t)$. Besides, its space complexity is $O(mn)$, which is the same as Algorithm 5.

There are several major differences between Algorithm 6 and nmAPG. First, the proximal step of Algorithm 6 is only inexact. To make the algorithm more robust, we do not allow nonmonotonous update (i.e., $F(\mathbf{X}_{t+1})$ cannot be larger than $F(\mathbf{X}_t)$). Moreover, we use a simpler acceleration scheme (step 4), in which only \mathbf{X}_t and \mathbf{X}_{t-1} are involved. On matrix completion problems, this allows using the “sparse plus low-rank” structure [14], [15] to greatly reduce the iteration complexity (Section 4.1). Finally, we do not require extra comparison of the objective at step 10. This further reduces the iteration complexity.

Algorithm 6 Accelerated FaNCL algorithm (FaNCL-acc).

Input: choose $\tau > \rho$, $\lambda_0 > \lambda$, $\delta > 0$ and $\nu \in (0, 1)$;

- 1: initialize $\mathbf{V}_0, \mathbf{V}_1 \in \mathbb{R}^n$ as random Gaussian matrices, $\mathbf{X}_0 = \mathbf{X}_1 = \mathbf{0}$ and $\alpha_0 = \alpha_1 = 1$;
 - 2: **for** $t = 1, 2, \dots, T$ **do**
 - 3: $\lambda_t = (\lambda_{t-1} - \lambda)\nu + \lambda$;
 - 4: $\mathbf{Y}_t = \mathbf{X}_t + \frac{\alpha_{t-1}-1}{\alpha_t}(\mathbf{X}_t - \mathbf{X}_{t-1})$;
 - 5: $\mathbf{R}_t = \text{QR}([\mathbf{V}_t, \mathbf{V}_{t-1}])$; // warm start
 - 6: $\mathbf{X}_{t+1}^a = \text{InexactPS}(\mathbf{Y}_t, \mathbf{R}_t)$;
 - 7: **if** $F(\mathbf{X}_{t+1}^a) \leq F(\mathbf{X}_t) - \frac{\delta}{2}\|\mathbf{X}_{t+1}^a - \mathbf{Y}_t\|_F^2$ **then**
 - 8: $\mathbf{X}_{t+1} = \mathbf{X}_{t+1}^a$;
 - 9: **else**
 - 10: $\mathbf{X}_{t+1} = \text{InexactPS}(\mathbf{X}_t, \mathbf{R}_t)$;
 - 11: **end if**
 - 12: $\alpha_{t+1} = \frac{1}{2}(\sqrt{4\alpha_t^2 + 1} + 1)$;
 - 13: **end for**
 - 14: **return** \mathbf{X}_{T+1} .
-

The following Proposition shows that Algorithm 6 generates a bounded sequence. Proof can be found in Appendix C.9.

Proposition 3.10. The sequence $\{\mathbf{X}_t\}$ generated from Algorithm 6 is bounded, and has at least one limit point.

In Corollary 3.8, $\|\mathbf{X}_{t+1} - \mathbf{X}_t\|_F^2$ is used to measure progress before and after the proximal step. In Algorithm 6, the proximal step may use the accelerated iterate \mathbf{Y}_t or the non-accelerated iterate \mathbf{X}_t . Hence, we use $\|\mathbf{X}_{t+1} - \mathbf{C}_t\|_F^2$, where $\mathbf{C}_t = \mathbf{Y}_t$ if step 8 is performed, and $\mathbf{C}_t = \mathbf{X}_t$ otherwise. Similar to Corollary 3.8, the following shows a $O(1/T)$ convergence rate. Proof can be found in Appendix C.10.

Corollary 3.11. For Algorithm 6, $\min_{t=1,\dots,T} \|\mathbf{X}_{t+1} - \mathbf{C}_t\|_F^2 \leq \frac{F(\mathbf{X}_1) - \inf F}{\min(c_1, \delta/2)T}$.

On nonconvex optimization problems, the optimal convergence rate for first-order methods is $O(1/T)$ [31], [40]. Thus, the convergence rate of Algorithm 6 (Corollary 3.11) cannot improve that of Algorithm 5 (Corollary 3.8). However, in practice, acceleration can still significantly reduce the number of iterations on nonconvex problems [25], [31]. On the other hand, as Algorithm 6 may need a second proximal step (step 10), its iteration time complexity can be higher than that of Algorithm 5. However, this is much compensated by the speedup in convergence. As will be demonstrated in Section 6.1, empirically Algorithm 6 is much faster.

The following Theorem shows that any limit point of the iterates from Algorithm 6 is also a critical point. Proof can be found in Appendix C.11.

Theorem 3.12. *Let $\{\mathbf{X}_{t_j}\}$ be a subsequence of $\{\mathbf{X}_t\}$ generated by Algorithm 6 such that $\lim_{t_j \rightarrow \infty} \mathbf{X}_{t_j} = \mathbf{X}_*$. With the assumption in Theorem 3.9, \mathbf{X}_* is a critical point of (1).*

4 APPLICATIONS

In this section, we consider two important instances of problem (1), namely, matrix completion [1] and robust principal component analysis (RPCA) [7]. As the accelerated FaNCL algorithm (Algorithm 6) is usually faster than its non-accelerated variant, we will only consider the accelerated variant here. For matrix completion (Section 4.1), we will show that Algorithm 6 can be made even faster and require much less memory by using the “sparse plus low-rank” structure of the problem. In Section 4.2, we show how Algorithm 6 can be extended to deal with the two parameter blocks in RPCA.

4.1 Matrix Completion

Matrix completion attempts to recover a low-rank matrix $\mathbf{O} \in \mathbb{R}^{m \times n}$ by observing only some of its elements [1]. Let the observed positions be indicated by $\Omega \in \{0, 1\}^{m \times n}$, such that $\Omega_{ij} = 1$ if O_{ij} is observed, and 0 otherwise. Matrix completion can be formulated as an optimization problem in (1), with

$$F(\mathbf{X}) = \frac{1}{2} \|\mathcal{P}_\Omega(\mathbf{X} - \mathbf{O})\|_F^2 + \lambda r(\mathbf{X}), \quad (6)$$

where $[\mathcal{P}_\Omega(\mathbf{A})]_{ij} = A_{ij}$ if $\Omega_{ij} = 1$ and 0 otherwise. In the following, we show that the time and space complexities of Algorithm 6 can be further reduced.

4.1.1 Utilizing the Problem Structure

First, consider step 7, which checks the objectives. Computing $F(\mathbf{X}_t)$ relies only on the observed positions in Ω and the singular values of \mathbf{X}_t . Hence, instead of explicitly constructing \mathbf{X}_t , we maintain the SVD $\mathbf{U}_t \Sigma_t \mathbf{V}_t^\top$ of \mathbf{X}_t and a sparse matrix $\mathcal{P}_\Omega(\mathbf{X}_t)$. Computing $F(\mathbf{X}_t)$ then takes $O(\|\Omega\|_1 k_t)$ time. Computing $F(\mathbf{X}_{t+1}^a)$ takes $O(\|\Omega\|_1 k_t)$ time, as \mathbf{R}_t has rank k_t . Next, since \mathbf{Y}_t is a linear combination of \mathbf{X}_t and \mathbf{X}_{t-1} in step 4, we can use the above SVD-factorized form and compute $\|\mathbf{X}_{t+1}^a - \mathbf{Y}_t\|_F^2$ in $O((m+n)k_t^2)$ time. Thus, step 7 then takes $O(\|\Omega\|_1 k_t + (m+n)k_t^2)$ time.

Steps 6 and 10 perform inexact proximal step. For the first proximal step (step 6), \mathbf{Y}_t (defined in step 4) can be rewritten as $(1 + \beta_t)\mathbf{X}_t - \beta_t\mathbf{X}_{t-1}$, where $\beta_t = (\alpha_{t-1} - 1)/\alpha_t$. When it calls InexactPS, step 1 of Algorithm 4 has

$$\begin{aligned} \mathbf{A} &= \mathbf{Y}_t + \frac{1}{\tau} \mathcal{P}_\Omega(\mathbf{Y}_t - \mathbf{O}) \\ &= (1 + \beta_t)\mathbf{X}_t - \beta_t\mathbf{X}_{t-1} + \frac{1}{\tau} \mathcal{P}_\Omega(\mathbf{Y}_t - \mathbf{O}). \end{aligned} \quad (7)$$

The first two terms involve low-rank matrices, while the last term involves a sparse matrix. This special “sparse plus low-rank” structure [14], [15] can speed up matrix

multiplications. Specifically, for any $\mathbf{V} \in \mathbb{R}^{n \times k}$, $\mathbf{A}\mathbf{V}$ can be obtained as

$$\begin{aligned} \mathbf{A}\mathbf{V} &= (1 + \beta_t)\mathbf{U}_t \Sigma_t (\mathbf{V}_t^\top \mathbf{V}) - \beta_t \mathbf{U}_{t-1} \Sigma_{t-1} (\mathbf{V}_{t-1}^\top \mathbf{V}) \\ &\quad + \frac{1}{\tau} \mathcal{P}_\Omega(\mathbf{O} - \mathbf{Y}_t) \mathbf{V}. \end{aligned} \quad (8)$$

Similarly, for any $\mathbf{U} \in \mathbb{R}^{m \times k}$, $\mathbf{U}^\top \mathbf{A}$ can be obtained as

$$\begin{aligned} \mathbf{U}^\top \mathbf{A} &= (1 + \beta_t)(\mathbf{U}^\top \mathbf{U}_t) \Sigma_t \mathbf{V}_t^\top - \beta_t (\mathbf{U}^\top \mathbf{U}_{t-1}) \Sigma_{t-1} \mathbf{V}_{t-1}^\top \\ &\quad + \frac{1}{\tau} \mathbf{U}^\top \mathcal{P}_\Omega(\mathbf{O} - \mathbf{Y}_t). \end{aligned} \quad (9)$$

Both (8) and (9) take $O((m+n)k_t k + \|\Omega\|_1 k)$ time (instead of $O(mnk_t)$). As \mathbf{R}_t in step 5 of Algorithm 6 has k_t columns, each call to approximate GSVT takes $O((m+n)k_t^2 + \|\Omega\|_1 k_t)$ time [15] (instead of $O(mnk_t)$). Finally, step 5 in Algorithm 4 also takes $O((m+n)k_t^2 + \|\Omega\|_1 k_t)$ time. As a result, step 6 of Algorithm 6 takes a total of $O((m+n)k_t^2 + \|\Omega\|_1 k_t)$ time. Step 10 is slightly cheaper (as no \mathbf{X}_{t-1} is involved), and its time complexity is $O((m+n)r_t k_t + \|\Omega\|_1 r_t)$. Summarizing, the iteration time complexity of Algorithm 6 is

$$O((m+n)k_t^2 + \|\Omega\|_1 k_t). \quad (10)$$

Usually, $k_t \ll n$ and $\|\Omega\|_1 \ll mn$ [1], [14]. Thus, (10) is much cheaper than the $O(mnk_t)$ complexity of standard FaNCL-acc (Section 3.6).

The space complexity is also reduced. We only need to store the low-rank factorizations of \mathbf{X}_t and \mathbf{X}_{t-1} , and the sparse matrices $\mathcal{P}_\Omega(\mathbf{X}_t)$ and $\mathcal{P}_\Omega(\mathbf{X}_{t-1})$. These take a total of $O((m+n)k_t + \|\Omega\|_1)$ space (instead of $O(mn)$ in Section 3.6).

These techniques can also be used on Algorithm 5. It can be easily shown that its iteration time complexity is $O((m+n)r_t k_t + \|\Omega\|_1 r_t)$, and its space complexity is $O((m+n)r_t + \|\Omega\|_1)$ (as no \mathbf{X}_{t-1} is involved).

4.1.2 Comparison with Existing Algorithms

Table 2 compares the convergence rates iteration time complexities, and space complexities of various matrix completion algorithms that will be empirically compared in Section 6. Overall, the proposed algorithms (Algorithms 5 and 6) enjoy fast convergence, cheap iteration complexity and low memory cost. While Algorithms 5 and 6 have the same convergence rate, we will see in Section 6.1 that Algorithm 6 (which uses acceleration) is significantly faster.

4.2 Robust Principal Component Analysis (RPCA)

Given a noisy data matrix $\mathbf{O} \in \mathbb{R}^{m \times n}$, RPCA assumes that \mathbf{O} can be approximated by the sum of a low-rank matrix \mathbf{X} plus some sparse noise \mathbf{S} [7]. Its optimization problem is:

$$\min_{\mathbf{X}, \mathbf{S}} F(\mathbf{X}, \mathbf{S}) \equiv f(\mathbf{X}, \mathbf{S}) + \lambda r(\mathbf{X}) + \nu g(\mathbf{S}), \quad (11)$$

where $f(\mathbf{X}, \mathbf{S}) = \frac{1}{2} \|\mathbf{X} + \mathbf{S} - \mathbf{O}\|_F^2$, r is a low-rank regularizer, and g is a sparsity-inducing regularizer. Here, we allow both r and g to be nonconvex and nonsmooth. Thus, (11) can be seen as a nonconvex extension of RPCA (which uses the nuclear norm regularizer for r and ℓ_1 -regularizer for g). Some examples of nonconvex r are shown in Table 1, and examples of nonconvex g include the ℓ_1 -norm, capped- ℓ_1 -norm [18] and log-sum-penalty [19].

TABLE 2

Comparison of the iteration time complexities, convergence rates and space complexity of various matrix completion solvers. Here, $k_t = r_t + r_{t-1}$, $\nu \in (0, 1)$ and integer $T_a > 0$ are constants. For the active subspace selection method (active) [17], T_s is the number of inner iterations required.

regularizer	method	convergence rate	iteration time complexity	space complexity
(convex) nuclear norm	APG [13], [34]	$O(1/T^2)$	$O(mnr_t)$	$O(mn)$
	active [17]	$O(\nu^{T-T_a})$	$O(\ \Omega\ _1 k_t T_s)$	$O((m+n)k_t + \ \Omega\ _1)$
	AIS-Impute [15]	$O(1/T^2)$	$O(\ \Omega\ _1 k_t + (m+n)k_t^2)$	$O((m+n)k_t + \ \Omega\ _1)$
fixed-rank factorization	LMAFit [41]	—	$O(\ \Omega\ _1 r_t + (m+n)r_t^2)$	$O((m+n)r_t + \ \Omega\ _1)$
	ER1MP [42]	$O(\nu^T)$	$O(\ \Omega\ _1)$	$O((m+n)r_t + \ \Omega\ _1)$
nonconvex	IRNN [5]	—	$O(mn^2)$	$O(mn)$
	GPG [26]	—	$O(mn^2)$	$O(mn)$
	FaNCL	$O(1/T)$	$O(\ \Omega\ _1 r_t + (m+n)r_t k_t)$	$O((m+n)r_t + \ \Omega\ _1)$
	FaNCL-acc	$O(1/T)$	$O(\ \Omega\ _1 k_t + (m+n)k_t^2)$	$O((m+n)k_t + \ \Omega\ _1)$

While (11) involves two blocks of parameters (\mathbf{X} and \mathbf{S}), they are not coupled together. Thus, we can use the separable property of proximal operator [29]:

$$\text{prox}_{\lambda r + \nu g}([\mathbf{X}, \mathbf{S}]) = [\text{prox}_{\lambda r}(\mathbf{X}), \text{prox}_{\nu g}(\mathbf{S})].$$

For many popular sparsity-inducing regularizers, computing $\text{prox}_{\nu g}(\mathbf{S})$ takes only $O(mn)$ time [24]. For example, when $g(\mathbf{S}) = \sum_{i,j} |S_{ij}|$, $[\text{prox}_{\nu g}(\mathbf{S})]_{ij} = \text{sign}(S_{ij}) \max(|S_{ij}| - \nu, 0)$, where $\text{sign}(x)$ is the sign of x . However, directly computing $\text{prox}_{\lambda r}(\mathbf{X})$ requires $O(mn^2)$ time and is expensive. To alleviate this problem, Algorithm 5 can be easily extended to Algorithm 7. The iteration time complexity, which is dominated by the inexact proximal steps in steps 6 and 13, is reduced to $O(mnk_t)$.

Algorithm 7 FaNCL-acc algorithm for RPCA.

Input: choose $\tau > \rho$, $\lambda_0 > \lambda$, $\delta > 0$, $\nu \in (0, 1)$ and $c_1 = \frac{\tau - \rho}{4}$;

- 1: initialize $\mathbf{V}_0, \mathbf{V}_1 \in \mathbb{R}^n$ as random Gaussian matrices, $\mathbf{X}_0 = \mathbf{X}_1 = \mathbf{0}$, $\mathbf{S}_0 = \mathbf{S}_1 = \mathbf{0}$ and $\alpha_0 = \alpha_1 = 1$;
- 2: **for** $t = 1, 2, \dots, T$ **do**
- 3: $\lambda_t = (\lambda_{t-1} - \lambda)\nu + \lambda$;
- 4: $[\mathbf{Y}_t^{\mathbf{X}}, \mathbf{Y}_t^{\mathbf{S}}] = [\mathbf{X}_t, \mathbf{S}_t] + \frac{\alpha_{t-1} - 1}{\alpha_t} ([\mathbf{X}_{t-1}, \mathbf{S}_{t-1}])$;
- 5: $\mathbf{R}_t = \text{QR}([\mathbf{V}_t, \mathbf{V}_{t-1}])$; // warm start
- 6: $\mathbf{X}_{t+1}^a = \text{InexactPS}(\mathbf{Y}_t^{\mathbf{X}}, \mathbf{R}_t)$;
- 7: $\mathbf{S}_{t+1}^a = \text{prox}_{\frac{\nu}{\tau} g}(\mathbf{Y}_t^{\mathbf{S}} - \frac{1}{\tau} \nabla_{\mathbf{S}} f(\mathbf{Y}_t^{\mathbf{X}}, \mathbf{Y}_t^{\mathbf{S}}))$;
- 8: $\Delta_t = \|\mathbf{X}_{t+1}^a - \mathbf{Y}_t^{\mathbf{X}}\|_F^2 + \|\mathbf{S}_{t+1}^a - \mathbf{Y}_t^{\mathbf{S}}\|_F^2$;
- 9: **if** $F(\mathbf{X}_{t+1}^a, \mathbf{S}_{t+1}^a) \leq F(\mathbf{X}_t, \mathbf{S}_t) - \frac{\delta}{2} \Delta_t$ **then**
- 10: $\mathbf{X}_{t+1} = \mathbf{X}_{t+1}^a$;
- 11: $\mathbf{S}_{t+1} = \mathbf{S}_{t+1}^a$;
- 12: **else**
- 13: $\mathbf{X}_{t+1} = \text{InexactPS}(\mathbf{X}_t, \mathbf{R}_t)$;
- 14: $\mathbf{S}_{t+1} = \text{prox}_{\frac{\nu}{\tau} g}(\mathbf{S}_t - \frac{1}{\tau} \nabla_{\mathbf{S}} f(\mathbf{X}_t, \mathbf{S}_t))$;
- 15: **end if**
- 16: $\alpha_{t+1} = \frac{1}{2}(\sqrt{4\alpha_t^2 + 1} + 1)$;
- 17: **end for**
- 18: **return** \mathbf{X}_{T+1} and \mathbf{S}_{T+1} .

Convergence results in Section 3.6 can be easily extended to this RPCA problem. Proofs of the following can be found in Appendices C.12, C.13, and C.14.

Proposition 4.1. *The sequence $\{[\mathbf{X}_t, \mathbf{S}_t]\}$ generated from Algorithm 7 is bounded, and has at least one limit point.*

Corollary 4.2. *Let $\mathbf{C}_t = [\mathbf{Y}_t^{\mathbf{X}}, \mathbf{Y}_t^{\mathbf{S}}]$ if steps 10 and 11 are performed, and $\mathbf{C}_t = [\mathbf{X}_t, \mathbf{S}_t]$ otherwise. Then, $\min_{t=1, \dots, T} \|\mathbf{X}_{t+1}, \mathbf{S}_{t+1}\| - \mathbf{C}_t\|_F^2 \leq \frac{F(\mathbf{X}_1, \mathbf{S}_1) - \inf F}{\min(c_1, \delta/2)T}$.*

Theorem 4.3. *Let $\{[\mathbf{X}_{t_j}, \mathbf{S}_{t_j}]\}$ be a subsequence of $\{[\mathbf{X}_t, \mathbf{S}_t]\}$ generated by Algorithm 6 such that $\lim_{t_j \rightarrow \infty} \mathbf{X}_{t_j} = \mathbf{X}_*$ and $\lim_{t_j \rightarrow \infty} \mathbf{S}_{t_j} = \mathbf{S}_*$. With the assumption in Theorem 3.9, $[\mathbf{X}_*, \mathbf{S}_*]$ is a critical point of (11).*

5 PARALLEL FANCL FOR MATRIX COMPLETION

In this section, we show how the proposed algorithms can be parallelized. We will only consider the matrix completion problem in (6). Extension to other problems, such as RPCA in Section 4.2, can be similarly performed. Moreover, for simplicity of discussion, we focus on the simpler FaNCL algorithm (Algorithm 5). Its accelerated variant (Algorithm 6) can be similarly parallelized and is shown in Appendix A.

Parallel algorithms for matrix completion have been proposed in [43], [44], [45]. However, they are based on stochastic gradient descent and matrix factorization, and cannot be directly used here.

5.1 Proposed Algorithm

Operations on a matrix \mathbf{X} are often of the form: (i) multiplications $\mathbf{U}^\top \mathbf{X}$ and \mathbf{XV} for some \mathbf{U}, \mathbf{V} (e.g., in (8), (9)); and (ii) element-wise operation (e.g., evaluation of $F(\mathbf{X})$ in (5)). A popular scheme in parallel linear algebra is block distribution [46]. Assume that there are q threads for parallelization. Block distribution partitions the rows and columns of \mathbf{X} into q parts, leading to a total of q^2 blocks. Figure 1 shows how computations of \mathbf{XV} , $\mathbf{U}^\top \mathbf{X}$ and element-wise operation can be easily parallelized. In Algorithm 5, the most important variables are the low-rank factorized form $\mathbf{U}_t \Sigma_t \mathbf{V}_t^\top$ of \mathbf{X}_t , and the sparse matrices $\mathcal{P}_\Omega(\mathbf{X}_t), \mathcal{P}_\Omega(\mathbf{O})$. Using block distribution, they are thus partitioned as in Figure 2.

The resultant parallelized version of FaNCL is shown in Algorithm 8. Steps that can be parallelized are marked with “ \triangleright ”. Two new subroutines are introduced, namely, **IndeSpan-PL** (step 6) which replaces QR factorization, and **ApproxGSVT-PL** (step 9) which is the parallelized version of Algorithm 3. They will be discussed in more detail in the following Sections. Note that Algorithm 8 is equivalent to Algorithm 5 except that it is parallelized. Thus, the convergence results in Section 3.5 still hold.

5.1.1 Identifying the Span (Step 5)

In step 4 of Algorithm 5, QR factorization is used to find the span of matrix $[\mathbf{V}_t, \mathbf{V}_{t-1}]$. This can be parallelized with the Householder transformation and Gaussian elimination [46], which however is typically very complex. The following

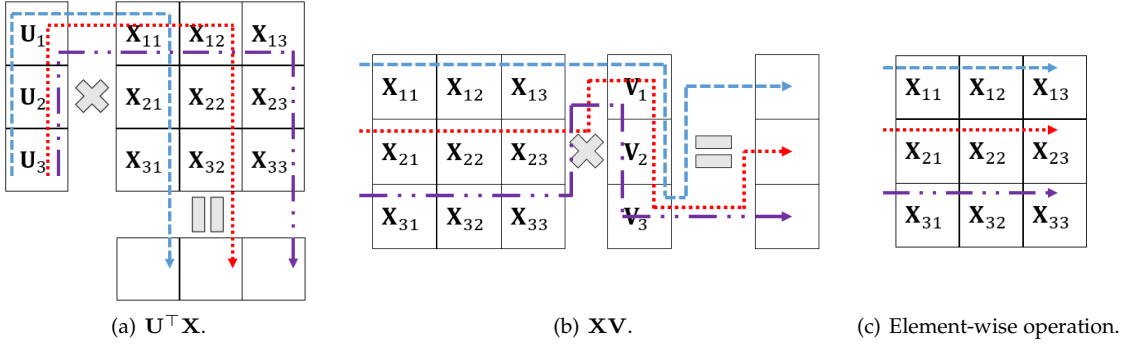


Fig. 1. Parallelization of different matrix operations. Here, the number of threads q is equal to 3. Each dotted path denotes operation of a thread.

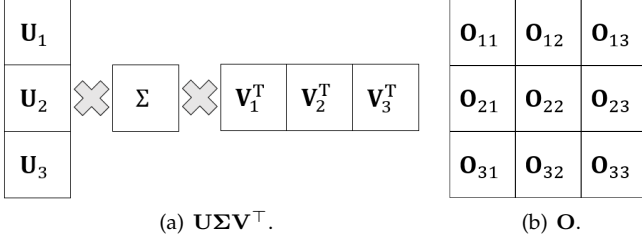


Fig. 2. Partitioning of variables $U\Sigma V^T$ and O , and three threads are used ($q = 3$).

Algorithm 8 FaNCL in parallel: FaNCL-PL.

Input: choose $\tau > \rho$, $\lambda_0 > \lambda$ and $\nu \in (0, 1)$;

- 1: initialize $V_0, V_1 \in \mathbb{R}^n$ as random Gaussian matrices and $X_1 = 0$;
- 2: partition $X_1, \mathcal{P}_\Omega(X_1)$ and $\mathcal{P}_\Omega(O)$;
- 3: start q threads for parallelization;
- 4: **for** $t = 1, 2, \dots, T$ **do**
- 5: $\lambda_t = (\lambda_{t-1} - \lambda)\nu^t + \lambda$;
- 6: $\triangleright R_t = \text{IndeSpan-PL}([V_t, V_{t-1}])$;
- 7: $\triangleright A_t = X_t - \frac{1}{\tau} \mathcal{P}_\Omega(X_t - O)$;
- 8: **for** $p = 1, 2, \dots$ **do**
- 9: $\triangleright [\tilde{X}_p, R_t] = \text{ApproxGSVT-PL}(A_t, R_t, \frac{\lambda}{\tau})$;
- 10: $\triangleright a_p = F(\tilde{X}_p)$;
- 11: $\triangleright a_t = F(X_t)$;
- 12: $\triangleright a_F = \|\tilde{X}_p - X_t\|_F^2$;
- 13: **if** $a_p \leq a_t - c_1 a_F$ **then**
- 14: **break**;
- 15: **end if**
- 16: **end for**
- 17: $\triangleright X_{t+1} = \tilde{X}_p$;
- 18: **end for**
- 19: **return** X_{T+1} .

Proposition proposes a simpler method to identify the span of a matrix. Proof can be found in Appendix C.15.

Proposition 5.1. *Given a matrix A , let the SVD of $A^T A$ be $V\Sigma V^T$, $w = [w_i]$ where $w_i = \Sigma_{ii}$ if $\Sigma_{ii} > 0$ and 1 otherwise. Then, $AV(\text{Diag}(w))^{-\frac{1}{2}}$ is orthogonal and contains $\text{span}(A)$.*

The resultant parallel algorithm is shown in Algorithm 9. Its time complexity is $O((\frac{n}{q} + q)k^2 + k^3)$. Algorithm 8 calls Algorithm 9 with input $[V_t, V_{t-1}]$, and thus takes $O((\frac{n}{q} + q)k_t^2 + k_t^3)$ time, where $k_t = r_t + r_{t-1}$. We do not parallelize steps 2-4, as only $k \times k$ matrices are involved and k is small.

Moreover, though step 3 uses SVD it only takes $O(k^3)$ time.

Algorithm 9 Parallel algorithm to identify the span of A : IndeSpan-PL(A).

Input: matrix $A \in \mathbb{R}^{n \times k}$;

- 1: $\triangleright B = A^T A$;
- 2: $[U, \Sigma, V] = \text{SVD}(B)$;
- 3: construct w as in Proposition 5.1;
- 4: $V = V\text{Diag}(w)$;
- 5: $\triangleright Q = AV$;
- 6: **return** Q . // $Q = [Q_1^T, \dots, Q_p^T]^T$

5.1.2 Approximate GSVT (Step 8)

The key steps in approximate GSVT (Algorithm 3) are the power method and SVD. The power method can be parallelized straightforwardly as in Algorithm 10, in which we also replace the QR subroutine with Algorithm 9.

Algorithm 10 Parallel power method: Powermethod-PL(Z, R).

Input: matrix $Z \in \mathbb{R}^{m \times n}$, $R \in \mathbb{R}^{n \times k}$.

- 1: $\triangleright Y_1 = ZR$;
- 2: **for** $j = 1, 2, \dots, J$ **do**
- 3: $\triangleright Q_j = \text{IndeSpan-PL}(Y_j)$;
- 4: $\triangleright Y_{j+1} = Z(Z^T Q_j)$;
- 5: **end for**
- 6: **return** Q_J .

As for SVD, multiple QR factorizations are usually needed for parallelization [46], which are complex as discussed in Section 5.1.1. The following Proposition performs it in a simpler manner. Proof can be found in Appendix C.16.

Proposition 5.2. *Given a matrix $B \in \mathbb{R}^{n \times k}$, let $P \in \mathbb{R}^{n \times k}$ be orthogonal and equals $\text{span}(B)$, and the SVD of $P^T B$ be $U\Sigma V^T$. Then, the SVD of B is $(PU)\Sigma V$.*

The resultant parallelized procedure for approximate GSVT is shown in Algorithm 11. At step 5, a small SVD is performed (by a single thread) on the $k \times k$ matrix $P^T B$. At step 8 of Algorithm 8, \tilde{X}_p is returned from Algorithm 11, and we keep \tilde{X}_p in its low-rank factorized form. Besides, when Algorithm 11 is called, $Z = A_t$ and has the “sparse plus low-rank” structure mentioned earlier. Hence, (8) and (9) can be used to speed up matrix multiplications². As R_t has k_t columns in Algorithm 8,

2. As no acceleration is used, β_t is equal to 0 in these two equations.

PowerMethod-PL in step 1 takes $O(\frac{k_t}{q}\|\Omega\|_1 + \frac{m+n}{q}k_t^2)$ time, steps 2-6 take $O((\frac{n}{q} + q)k_t^2 + k_t^3)$ time, and the rest takes $O(k_t)$ time. The total time complexity for Algorithm 11 is $O(\frac{k_t}{q}\|\Omega\|_1 + \frac{m+n}{q}k_t^2 + (q + k_t)k_t^2)$.

Algorithm 11 Approximate GSVT in parallel: ApproxGSVT-PL($\mathbf{Z}, \mathbf{R}, \mu$).

Input: partitioned matrix $\mathbf{Z} \in \mathbb{R}^{m \times n}$ and $\mathbf{R} \in \mathbb{R}^{n \times k}$;
 1: $\triangleright \mathbf{Q} = \text{PowerMethod-PL}(\mathbf{Z}, \mathbf{R})$;
 2: $\triangleright \mathbf{B} = \mathbf{Z}^\top \mathbf{Q}$; // $\mathbf{B} \in \mathbb{R}^{n \times k}$
 3: $\triangleright \mathbf{P} = \text{Iden-Span}(\mathbf{B})$;
 4: $\triangleright \mathbf{A} = \mathbf{P}^\top \mathbf{B}$;
 5: $[\mathbf{U}, \Sigma, \mathbf{V}] = \text{SVD}(\mathbf{A})$; // $\mathbf{U}, \Sigma, \mathbf{V}, \mathbf{A} \in \mathbb{R}^{k \times k}$
 6: $\triangleright \mathbf{U} = \mathbf{P}\mathbf{U}$;
 7: $a = \text{number of } \Sigma_{ii}'\text{'s that are } > \gamma \text{ in Corollary 3.2}$;
 8: $\triangleright \mathbf{U}_a = a \text{ leading columns of } \mathbf{U}$;
 9: $\triangleright \mathbf{V}_a = a \text{ leading columns of } \mathbf{V}$;
 10: **for** $i = 1, 2, \dots, a$ **do**
 11: obtain y_i^* from (4);
 12: **end for**
 13: **return** the low-rank components of $\tilde{\mathbf{X}}$ ($\mathbf{Q}\mathbf{U}_a$, $\text{Diag}([y_1^*, \dots, y_a^*])$ and \mathbf{V}_a^\top), and \mathbf{V} .

5.1.3 Checking of Objectives (steps 9-11)

As shown in Figures 1(c), computation of $\|\mathcal{P}_\Omega(\mathbf{X}_t - \mathbf{O})\|_F^2$ in $F(\cdot)$ can be directly parallelized and takes $O(\frac{1}{p}\|\Omega\|_1)$ time. As r only relies on Σ_t , only one thread is needed to evaluate $r(\mathbf{X}_t)$. Thus, computing $F(\mathbf{X}_t)$ takes $O(\frac{r_t}{q}\|\Omega\|_1)$ time. Similarly, computing $F(\tilde{\mathbf{X}}_p)$ takes $O(\frac{k_t}{q}\|\Omega\|_1)$ time. As $\|\tilde{\mathbf{X}}_p - \mathbf{X}_t\|_F^2 = \text{tr}(\tilde{\mathbf{X}}_p^\top \tilde{\mathbf{X}}_p - 2\tilde{\mathbf{X}}_p^\top \mathbf{X}_t - \mathbf{X}_t^\top \mathbf{X}_t)$, the low-rank factorized forms of $\tilde{\mathbf{X}}_p$ and \mathbf{X}_t can be utilized. Based on Figures 1(a) and 1(b), it can be performed in $O(\frac{m+n}{q}k_t^2)$ time. Thus, the time complexity for steps 9-11 in Algorithm 8 is $O(\frac{k_t}{q}\|\Omega\|_1 + \frac{m+n}{q}k_t^2)$.

The iteration time complexity for Algorithm 8 is thus $O(\frac{1}{q}((m+n)k_t^2 + \|\Omega\|_1 k_t) + (q + k_t)k_t^2)$. Compared with (10), the speedup w.r.t. the number of threads q is almost linear.

6 EXPERIMENTS

In this section, we perform experiments on matrix completion, RPCA and the parallelized variant of Algorithm 6 (Appendix A). Experiments are performed on a Windows server 2013 system with Intel Xeon E5-2695-v2 CPU (12 cores, 2.4GHz) and 256GB memory. All the algorithms in Sections 6.1 and 6.2 are implemented in Matlab. For Section 6.3, we use C++, the Intel-MKL package³ for matrix operations, and the standard thread library⁴ for multi-thread programming.

6.1 Matrix Completion

We compare a number of low-rank matrix completion solvers, including models based on (i) the commonly used (convex) nuclear norm regularizer; (ii) fixed-rank factorization models [41], [42], which decompose the observed

matrix \mathbf{O} into a product of rank- k matrices \mathbf{U} and \mathbf{V} . Its optimization problem can be written as: $\min_{\mathbf{U}, \mathbf{V}} \frac{1}{2}\|\mathcal{P}_\Omega(\mathbf{UV} - \mathbf{O})\|_F^2 + \frac{\lambda}{2}(\|\mathbf{U}\|_F^2 + \|\mathbf{V}\|_F^2)$; and (iii) nonconvex regularizers, including the capped- ℓ_1 (with θ in Table 1 set to 2λ), LSP (with $\theta = \sqrt{\lambda}$), and TNN (with $\theta = 3$).

The nuclear norm minimization algorithms to be compared include:

- 1) Accelerated proximal gradient (APG) algorithm [13], [34], with the partial SVD by PROPACK [36];
- 2) AIS-Impute [14], an inexact and acceleration proximal algorithm. The “sparse plus low-rank” structure of the matrix iterate is utilized to speed up computation (Section 4.1); and
- 3) Active subspace selection (denoted “active”) [17], which adds/removes rank-one subspaces from the active set in each iteration. The nuclear norm optimization problem is then reduced to a smaller problem defined only on this active set.

We do not compare with the Frank-Wolfe algorithm [16] and stochastic gradient descent [47], as they have been shown to be less efficient [15], [17].

For the fixed-rank factorization models (where the rank is tuned by the validation set), we compare with the two state-of-the-art algorithms:

- 1) Low-rank matrix fitting (LMaFit) algorithm [41]; and
- 2) Economical rank-one matrix pursuit (ER1MP) [42], which pursues a rank-one basis in each iteration.

We do not compare with the concave-convex procedure [3], [18], since it has been shown to be inferior to IRNN [24].

For models with nonconvex low-rank regularizers, we compare with the following solvers:

- 1) Iterative reweighted nuclear norm (IRNN) [5];
- 2) Generalized proximal gradient (GPG) algorithm [26], with the underlying problem (4) solved using the closed-form solutions in [24]; and
- 3) The proposed FaNCL algorithm (Algorithm 5) and its accelerated variant FaNCL-acc (Algorithm 6). We set $J = 3$ and $p = 1$.

All the algorithms are stopped when the difference in objective values between consecutive iterations becomes smaller than 10^{-5} .

6.1.1 Synthetic Data

The observed $m \times m$ matrix is generated as $\mathbf{O} = \mathbf{UV} + \mathbf{G}$, where the elements of $\mathbf{U} \in \mathbb{R}^{m \times k}$, $\mathbf{V} \in \mathbb{R}^{k \times m}$ (with $k = 5$) are sampled i.i.d. from the standard normal distribution $\mathcal{N}(0, 1)$, and elements of \mathbf{G} sampled from $\mathcal{N}(0, 0.1)$. A total of $\|\Omega\|_1 = 2mk \log(m)$ random elements in \mathbf{O} are observed. Half of them are used for training, and the rest as validation set for parameter tuning. Testing is performed on the unobserved elements.

For performance evaluation, we use (i) the normalized mean squared error $\text{NMSE} = \|\mathcal{P}_{\Omega^\perp}(\mathbf{X} - \mathbf{UV})\|_F / \|\mathcal{P}_{\Omega^\perp}(\mathbf{UV})\|_F$, where \mathbf{X} is the recovered matrix and Ω^\perp denotes the unobserved positions; (ii) rank of \mathbf{X} ; and (iii) training CPU time. We vary m in the range $\{500, 1000, 2000\}$. Each experiment is repeated five times.

3. <https://software.intel.com/en-us/intel-mkl>

4. <http://www.cplusplus.com/reference/thread/thread/>

TABLE 3

Matrix completion performance on the synthetic data. Here, NMSE is scaled by 10^{-2} , CPU time is in seconds and the number in brackets is the data sparsity. The best results (according to the pairwise t-test with 95% confidence) are highlighted.

		$m = 500$ (12.43%)			$m = 1000$ (6.91%)			$m = 2000$ (3.80%)		
		NMSE	rank	time	NMSE	rank	time	NMSE	rank	time
nuclear norm	APG	4.26±0.01	50	12.6±0.7	4.27±0.01	61	99.6±9.1	4.13±0.01	77	1177.5±134.2
	AIS-Impute	4.11±0.01	55	5.8±2.9	4.01±0.03	57	37.9±2.9	3.50±0.01	65	338.1±54.1
	active	5.37±0.03	53	12.5±1.0	6.63±0.03	69	66.4±3.3	6.44±0.10	85	547.3±91.6
fixed rank	LMaFit	3.08±0.02	5	0.5±0.1	3.02±0.02	5	1.3±0.1	2.84±0.03	5	4.9±0.3
	ER1MP	21.75±0.05	40	0.3±0.1	21.94±0.09	54	0.8±0.1	20.38±0.06	70	2.5±0.3
capped ℓ_1	IRNN	1.98±0.01	5	14.5±0.7	1.99±0.01	5	146.0±2.6	1.79±0.01	5	2759.9±252.8
	GPG	1.98±0.01	5	14.8±0.9	1.99±0.01	5	144.6±3.1	1.79±0.01	5	2644.9±358.0
	FaNCL	1.97±0.01	5	0.3±0.1	1.98±0.01	5	1.0±0.1	1.79±0.01	5	5.0±0.4
	FaNCL-acc	1.97±0.01	5	0.1±0.1	1.95±0.01	5	0.5±0.1	1.78±0.01		2.3±0.2
LSP	IRNN	1.96±0.01	5	16.8±0.6	1.89±0.01	5	196.1±3.9	1.79±0.01	5	2951.7±361.3
	GPG	1.96±0.01	5	16.5±0.4	1.89±0.01	5	193.4±2.1	1.79±0.01	5	2908.9±358.0
	FaNCL	1.96±0.01	5	0.4±0.1	1.89±0.01	5	1.3±0.1	1.79±0.01	5	5.5±0.4
	FaNCL-acc	1.96±0.01	5	0.2±0.1	1.89±0.01	5	0.7±0.1	1.77±0.01		2.4±0.2
TNN	IRNN	1.96±0.01	5	18.8±0.6	1.88±0.01	5	223.1±4.9	1.77±0.01	5	3220.3±379.7
	GPG	1.96±0.01	5	18.0±0.6	1.88±0.01	5	220.9±4.5	1.77±0.01	5	3197.8±368.9
	FaNCL	1.95±0.01	5	0.4±0.1	1.88±0.01	5	1.4±0.1	1.77±0.01	5	6.1±0.5
	FaNCL-acc	1.96±0.01	5	0.2±0.1	1.88±0.01	5	0.8±0.1	1.77±0.01		2.9±0.2

Results are shown in Table 3. As can be seen, nonconvex regularization (capped- ℓ_1 , LSP and TNN) leads to much lower NMSE's than convex nuclear norm regularization and fixed-rank factorization. Moreover, the nuclear norm and ER1MP output much higher ranks. In terms of speed among the nonconvex low-rank solvers, FaNCL is fast, and FaNCL-acc is the fastest. The larger the matrix, the higher is the speedup of FaNCL and FaNCL-acc over GPG and IRNN.

6.1.2 MovieLens

Experiment is performed on the popular *MovieLens* data set (Table 4), which contain ratings of different users on movies. We follow the setup in [42], and use 50% of the observed ratings for training, 25% for validation and the rest for testing. For performance evaluation, we use the root mean squared error on the test set $\bar{\Omega}$: $\text{RMSE} = \sqrt{\|\mathcal{P}_{\bar{\Omega}}(\mathbf{X} - \mathbf{O})\|_F^2 / \|\bar{\Omega}\|_1}$, where \mathbf{X} is the recovered matrix. The experiment is repeated five times.

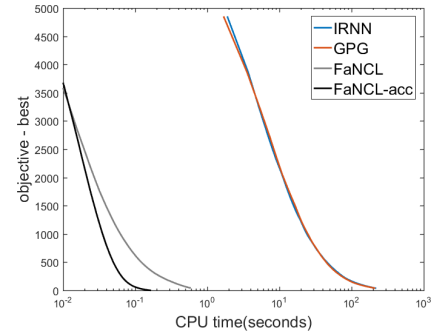
TABLE 4
Recommendation data sets used in the experiments.

		#users	#movies	#ratings
<i>MovieLens</i>	100K	943	1,682	100,000
	1M	6,040	3,449	999,714
	10M	69,878	10,677	10,000,054
<i>netflix</i>		480,189	17,770	100,480,507
<i>yahoo</i>		249,012	296,111	62,551,438

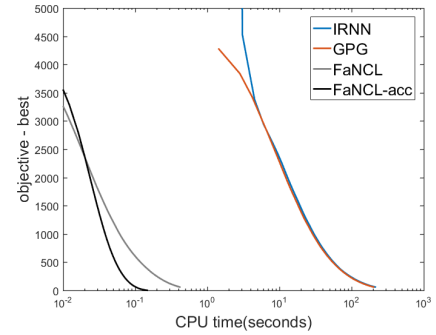
Results are shown in Table 5. Again, nonconvex regularizers lead to the lowest RMSE's. Moreover, FaNCL-acc is also the fastest among nonconvex low-rank solvers, even faster than the state-of-the-art GPG. In particular, FaNCL and its accelerated variant FaNCL-acc are the only solvers (for nonconvex regularization) that can be run on the *MovieLens*-1M and 10M data sets. Figure 3 compares the objectives vs CPU time for the nonconvex regularization solvers on *MovieLens*-100K. As can be seen, FaNCL and FaNCL-acc decrease the objective and RMSE much faster than the others. Figure 4 shows the testing RMSEs on *MovieLens*-10M. Again, FaNCL-acc is the fastest.

6.1.3 Netflix and Yahoo

Next, we perform experiments on two very large recommendation data sets, *Netflix* and *Yahoo* (Table 4). We randomly



(a) capped- ℓ_1 .



(b) LSP.

Fig. 3. Objective vs CPU time for the capped- ℓ_1 and LSP on *MovieLens*-100K. The plot of TNN is similar and thus not shown.

use 50% of the observed ratings for training, 25% for validation and the rest for testing. Each experiment is repeated five times.

Results are shown in Table 6. APG, GPG and IRNN cannot be run as the data set is large. AIS-Impute has similar running time as LMaFit but inferior performance, and thus is not compared. Again, the nonconvex regularizers converge faster, yield lower RMSE's and solutions of much lower ranks. Figure 5 shows the objectives and RMSE vs time, and FaNCL-acc is the fastest.⁵

5. On these two data sets, ER1MP easily overfits as the rank increases. Hence, the validation set selects a smaller rank (relative to that obtained by the nuclear norm) and ER1MP stops earlier. However, as can be seen, its RMSE is much worse.

TABLE 5

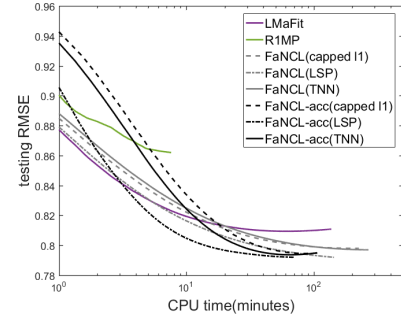
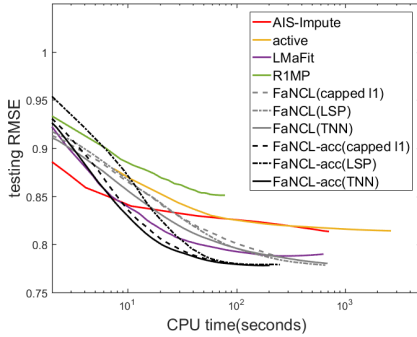
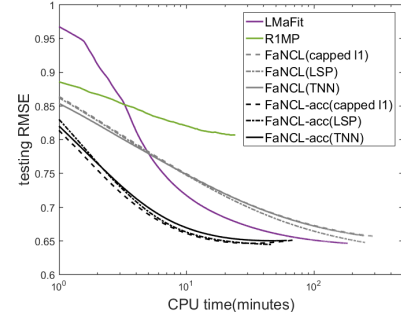
Matrix completion results on the *MovieLens* data sets (time is in seconds). The best results (according to the pairwise t-test with 95% confidence) are highlighted.

		<i>MovieLens-100K</i>			<i>MovieLens-1M</i>			<i>MovieLens-10M</i>		
		RMSE	rank	time	RMSE	rank	time	RMSE	rank	time
nuclear norm	APG	0.877±0.001	36	47.1±7.6	0.818±0.001	67	2174.4±117.3	—	—	> 10 ⁵
	AIS-Impute	0.878±0.002	36	1.2±0.1	0.819±0.001	67	12.4±0.9	0.813±0.001	100	540.6±107.9
	active	0.878±0.001	36	2.7±0.3	0.820±0.001	67	82.6±5.2	0.814±0.001	100	2338.3±304.7
fixed rank	LMaFit	0.865±0.002	2	1.2±0.2	0.806±0.003	6	24.8±1.3	0.792±0.001	9	501.7±95.2
	ER1MP	0.917±0.003	5	0.1±0.1	0.853±0.001	13	1.3±0.1	0.852±0.002	22	62.7±17.8
capped ℓ_1	IRNN	0.854±0.003	3	289.9±60.6	—	—	> 10 ⁴	—	—	> 10 ⁵
	GPG	0.855±0.002	3	223.6±49.7	—	—	> 10 ⁴	—	—	> 10 ⁵
	FaNCL	0.855±0.003	3	0.5±0.2	0.788±0.002	5	16.8±2.9	0.783±0.001	8	341.6±58.5
	FaNCL-acc	0.860±0.009	3	0.3±0.1	0.791±0.001	5	4.7±0.5	0.778±0.001	8	98.4±14.7
LSP	IRNN	0.856±0.001	2	286.6±48.1	—	—	> 10 ⁴	—	—	> 10 ⁵
	GPG	0.856±0.001	2	277.5±56.9	—	—	> 10 ⁴	—	—	> 10 ⁵
	FaNCL	0.856±0.001	2	0.5±0.1	0.786±0.001	5	24.6±1.5	0.779±0.001	9	641.4±82.6
	FaNCL-acc	0.853±0.001	2	0.2±0.1	0.787±0.001	5	5.4±0.5	0.779±0.001	9	209.3±42.5
TNN	IRNN	0.854±0.004	3	133.8±30.7	—	—	> 10 ⁴	—	—	> 10 ⁵
	GPG	0.853±0.005	3	591.3±127.2	—	—	> 10 ⁴	—	—	> 10 ⁵
	FaNCL	0.865±0.016	3	1.2±0.2	0.786±0.001	5	23.8±0.9	0.780±0.001	8	712.0±142.6
	FaNCL-acc	0.861±0.009	3	0.4±0.1	0.786±0.001	5	5.4±0.3	0.778±0.001	9	207.6±56.9

TABLE 6

Results on the *netflix* and *yahoo* data sets (CPU time is in minutes). The best results (according to the pairwise t-test with 95% confidence) are highlighted.

		<i>netflix</i>			<i>yahoo</i>		
		RMSE	rank	time	RMSE	rank	time
fixed rank	LMaFit	0.811±0.001	15	116.4±12.2	0.666±0.001	10	229.3±62.8
	ER1MP	0.862±0.006	25	7.1±1.1	0.810±0.003	77	27.9±7.5
capped- ℓ_1	FaNCL	0.798±0.001	13	220.0±24.0	0.656±0.001	8	333.0±113.9
	FaNCL-acc	0.795±0.001	13	92.8±13.8	0.651±0.001	8	90.2±16.2
LSP	FaNCL	0.794±0.001	15	145.5±10.2	0.652±0.001	9	339.8±93.9
	FaNCL-acc	0.792±0.001	15	69.6±21.1	0.650±0.001	8	76.1±33.2
TNN	FaNCL	0.797±0.001	13	275.1±16.7	0.657±0.001	7	321.2±69.1
	FaNCL-acc	0.795±0.001	13	104.3±17.1	0.650±0.001	7	72.9±16.1

(a) *netflix*.(b) *yahoo*.Fig. 5. RMSE vs CPU time on the *netflix* and *yahoo* data sets.

6.2 Robust Principal Component Analysis

6.2.1 Synthetic Data

In this section, we first perform experiments on a synthetic data set. The observed $m \times m$ matrix is generated as $\mathbf{O} = \mathbf{U}\mathbf{V} + \tilde{\mathbf{S}} + \mathbf{G}$, where elements of $\mathbf{U} \in \mathbb{R}^{m \times k}$, $\mathbf{V} \in \mathbb{R}^{k \times m}$ (with $k = 0.01m$) are sampled i.i.d. from $\mathcal{N}(0, 1)$, and elements of \mathbf{G} are sampled from $\mathcal{N}(0, 0.1)$. Matrix $\tilde{\mathbf{S}}$ is sparse, with 1% of its elements randomly set to $5\|\mathbf{U}\mathbf{V}\|_\infty$ or $-5\|\mathbf{U}\mathbf{V}\|_\infty$ with equal probabilities. The whole data set is then randomly split into training and test sets of equal size. The standard ℓ_1 regularizer is used as the sparsity regularizer g in (11), and different convex/nonconvex low-rank regularizers are used as r . Hyperparameters λ and ν in (11) are tuned using the training set.

For performance evaluation, we use (i) NMSE = $\|(\mathbf{X} + \mathbf{S}) - (\mathbf{U}\mathbf{V} + \tilde{\mathbf{S}})\|_F / \|\mathbf{U}\mathbf{V} + \tilde{\mathbf{S}}\|_F$, where \mathbf{X} and \mathbf{S} are the recovered low-rank and sparse components, respectively; (ii)

accuracy on locating the sparse support of $\tilde{\mathbf{S}}$ (i.e., percentage of entries that \hat{S}_{ij} and S_{ij} are nonzero or zero together); (iii) the recovered rank and (iv) CPU time. We vary m in $\{500, 1000, 2000\}$. Each experiment is repeated five times. Note that IRNN and active subspace selection cannot be

TABLE 7

RPCA performance on synthetic data. NMSE is scaled by 10^{-3} , and CPU time is in seconds. The best results (according to the pairwise t-test with 95% confidence) are highlighted.

		$m = 500$			$m = 1000$			$m = 2000$		
		NMSE	rank	time	NMSE	rank	time	NMSE	rank	time
nuclear norm	APG	4.88±0.17	5	4.3±0.2	3.31±0.06	10	24.5±1.0	2.40±0.05	20	281.2±26.7
capped- ℓ_1	GPG	4.51±0.16	5	8.5±2.6	2.93±0.07	10	42.9±6.6	2.16±0.05	20	614.1±64.7
	FaNCL-acc	4.51±0.16	5	0.8±0.2	2.93±0.07	10	2.8±0.1	2.16±0.05	20	24.9±2.0
LSP	GPG	4.51±0.16	5	8.3±2.3	2.93±0.07	10	42.6±5.9	2.16±0.05	20	638.8±72.6
	FaNCL-acc	4.51±0.16	5	0.8±0.1	2.93±0.07	10	2.9±0.1	2.16±0.05	20	26.6±4.1
TNN	GPG	4.51±0.16	5	8.5±2.4	2.93±0.07	10	43.2±5.8	2.16±0.05	20	640.7±59.1
	FaNCL-acc	4.51±0.16	5	0.8±0.1	2.93±0.07	10	2.9±0.1	2.16±0.05	20	26.9±2.7

TABLE 8

PSNR (in dB) and CPU time (in seconds) on the video background removal experiment. The PSNRs for all the input videos are 16.47dB.

		<i>bootstrap</i>		<i>campus</i>		<i>escalator</i>		<i>hall</i>	
		PSNR	time	PSNR	time	PSNR	time	PSNR	time
nuclear norm	APG	23.07±0.02	524±84	22.47±0.02	101±6	24.01±0.01	594±86	24.25±0.03	553±85
capped- ℓ_1	GPG	23.81±0.01	3122±284	23.21±0.02	691±43	24.62±0.02	5369±238	25.22±0.03	4841±255
	FaNCL-acc	24.05±0.01	193±18	23.24±0.02	53±5	24.68±0.02	242±22	25.22±0.03	150±10
LSP	GPG	23.93±0.03	1922±111	23.61±0.02	324±27	24.57±0.01	5053±369	25.37±0.03	2889±222
	FaNCL-acc	24.30±0.02	189±15	23.99±0.02	69±8	24.56±0.01	168±15	25.37±0.03	144±9
TNN	GPG	23.85±0.03	1296±203	23.12±0.02	671±21	24.60±0.01	4091±195	25.26±0.04	4709±367
	FaNCL-acc	24.12±0.02	203±11	23.14±0.02	49±5	24.66±0.01	254±30	25.25±0.06	148±11

used here. Their objectives are of the form “smooth function plus low-rank regularizer”, but RPCA also has a nonsmooth ℓ_1 regularizer. Similarly, AIS-Impute is only for matrix completion. Moreover, FaNCL, which has been shown to be slower than FaNCL-acc, will not be compared.

Results are shown in Table 7. The accuracies on locating the sparse support are always 100% for all methods, and thus are not shown. Moreover, while both convex and non-convex regularizers can perfectly recover the matrix rank and sparse locations, the nonconvex regularizers have lower NMSE’s. As in matrix completion, FaNCL-acc is much faster; the larger the matrix, the higher the speedup.

6.2.2 Background Removal on Videos

In this section, we use RPCA for background removal in videos. Four benchmark videos in [7], [8] are used (Table 9), and example frames are shown in Figure 6. As in [7], the image background is considered low-rank, while the foreground moving objects contribute to the sparse component.

TABLE 9
Videos used in the experiment.

	<i>bootstrap</i>	<i>campus</i>	<i>escalator</i>	<i>hall</i>
#pixels / frame	19,200	20,480	20,800	25,344
total #frames	9,165	4,317	10,251	10,752



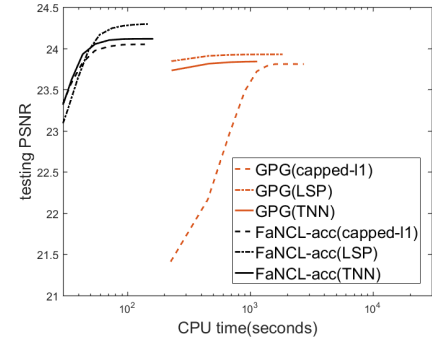
(a) *bootstrap*. (b) *campus*. (c) *escalator*. (d) *hall*.

Fig. 6. Example image frames in the videos.

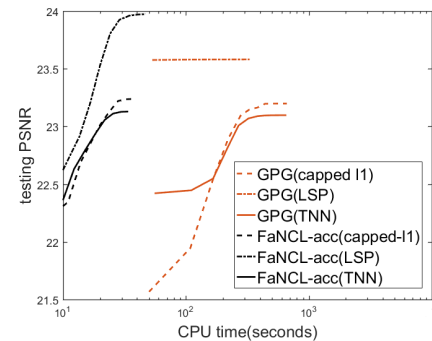
Given a video with n image frames, each $m_1 \times m_2$ frame is first reshaped as a m -dimensional column vector (where $m = m_1 m_2$), and then all the frames are stacked together to form a $m \times n$ matrix. The pixel values are normalized to $[0, 1]$, and Gaussian noise from $\mathcal{N}(0, 0.15)$ is added. The experiment is repeated five times. For performance evaluation, we use the commonly used peak signal-to-noise ratio

[6]: $\text{PSNR} = -10 \log_{10}(\frac{1}{mn} \|\mathbf{X} - \mathbf{O}\|_F^2)$ where $\mathbf{X} \in \mathbb{R}^{m \times n}$ is the recovered video, and $\mathbf{O} \in \mathbb{R}^{m \times n}$ is the ground-truth.

Results are shown in Table 8. As can be seen, the non-convex regularizers lead to better PSNR’s than the convex nuclear norm. Moreover, FaNCL-acc is much faster than GPG. Figure 7 shows PSNR vs CPU time on the *bootstrap* and *campus* data sets. Again, FaNCL-acc converges to higher PSNR much faster. Results on *hall* and *escalator* are similar.



(a) *bootstrap*.



(b) *campus*.

Fig. 7. PSNR vs CPU time on the *bootstrap* and *campus* videos.

6.3 Parallel Matrix Completion

In this section, we experiment with the proposed parallel algorithm in Section 5 on the *Netflix* and *Yahoo* data sets (Table 4). We do not compare with factorization-based

algorithms [44], [45], as they have inferior performance (Section 6.1). The machine has 12 cores, and we use one thread for each core. As suggested in [44], we randomly shuffle all the matrix columns and rows before partitioning. We use the LSP penalty (with $\theta = \sqrt{\lambda}$) and fix the total number of iterations to 250. The hyperparameters are the same as in Section 6.1.3. Experiments are repeated five times.

Convergence of the objective for a typical run is shown in Figure 8. As we have multiple threads running on a single CPU, we report the clock time instead of CPU time. As can be seen, the accelerated algorithms are much faster than the non-accelerated ones, and parallelization provides further speedup.

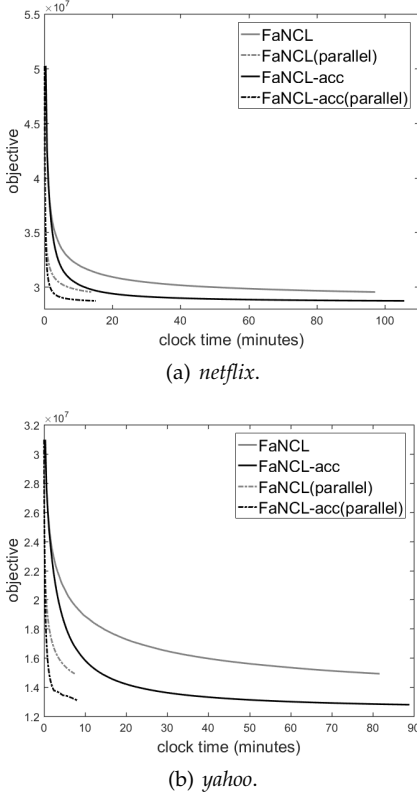


Fig. 8. Objective value vs clock time for the sequential/parallel versions of FaNCL on the *netflix* and *yahoo* data sets.

Figure 9 shows the speedup with different numbers of threads. As can be seen, the parallelized variants scale well with the number of threads. In particular, scaling is better on *yahoo*. The observed entries in its partitioned data submatrices are distributed more evenly, which improves performance of parallel algorithms [48]. Another observation is that the speedup can be larger than one. As discussed in [49], in performing multiplications with a large sparse matrix, a significant amount of time is spent on indexing its nonzero elements. When the matrix is partitioned, each submatrix becomes smaller and easier to be indexed. Thus, the memory cache also becomes more effective.

7 CONCLUSION

In this paper, we considered the challenging problem of nonconvex low-rank matrix optimization. The key observations are that for the popular low-rank regularizers, the singular values obtained from the proximal operator can

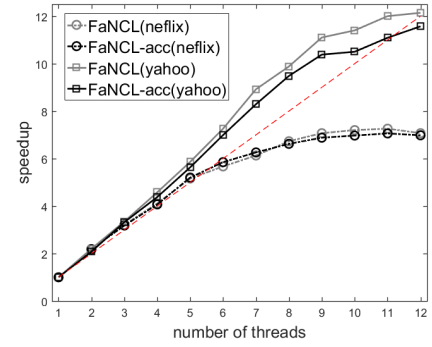


Fig. 9. Speedup vs the number of threads for parallel FaNCL. The red dashed line indicates linear speedup.

be automatically thresholded, and the proximal operator can be computed on a smaller matrix. This allows the proximal operator to be efficiently approximated by the power method. We extended the proximal algorithm in this nonconvex optimization setting with acceleration and inexact proximal step. We further parallelized the proposed algorithm, which scales well w.r.t. the number of threads. Extensive experiments on matrix completion and RPCA show that the proposed algorithm is much faster than the state-of-the-art. It also demonstrates that nonconvex low-rank regularizers outperform the standard (convex) nuclear norm regularizer.

In the parallel setting, typically the observed entries are non-uniformly distributed in the partitioned matrices, and so workloads in the different threads are not well balanced. One future direction is to allow asynchronized updates of the parallel algorithm. This can help to reduce the waiting time for threads with light workloads, and makes more efficient use of the CPU. Moreover, while parallel algorithms on multicore machines are easier to implement and do not have communication issues, they are less scalable than distributed algorithms [50]. To allow further scaleup to massive data sets, we will consider extending the proposed algorithms to a distributed computing environment.

REFERENCES

- [1] E. Candès and B. Recht, "Exact matrix completion via convex optimization," *Foundations of Computational Mathematics*, vol. 9, no. 6, pp. 717–772, 2009.
- [2] H. Ji, C. Liu, Z. Shen, and Y. Xu, "Robust video denoising using low rank matrix completion," in *Proceedings of the 23rd Conference on Computer Vision and Pattern Recognition*, 2010, pp. 1791–1798.
- [3] Y. Hu, D. Zhang, J. Ye, X. Li, and X. He, "Fast and accurate matrix completion via truncated nuclear norm regularization," *IEEE Transactions on Pattern Analysis and Machine Intelligence*, vol. 35, no. 9, pp. 2117–2130, 2013.
- [4] J. Liu, P. Musialski, P. Wonka, and J. Ye, "Tensor completion for estimating missing values in visual data," *IEEE Transactions on Pattern Analysis and Machine Intelligence*, vol. 35, no. 1, pp. 208–220, 2013.
- [5] C. Lu, J. Tang, S. Yan, and Z. Lin, "Nonconvex nonsmooth low rank minimization via iteratively reweighted nuclear norm," *IEEE Transactions on Image Processing*, vol. 25, no. 2, pp. 829–839, 2016.
- [6] S. Gu, Q. Xie, D. Meng, W. Zuo, X. Feng, and L. Zhang, "Weighted nuclear norm minimization and its applications to low level vision," *International Journal of Computer Vision*, vol. 121, no. 2, pp. 183–208, 2017.
- [7] E. Candès, X. Li, Y. Ma, and J. Wright, "Robust principal component analysis?" *Journal of the ACM*, vol. 58, no. 3, p. 11, 2011.

- [8] Q. Sun, S. Xiang, and J. Ye, "Robust principal component analysis via capped norms," in *Proceedings of the 19th International Conference on Knowledge Discovery and Data Mining*, 2013, pp. 311–319.
- [9] T.-H. Oh, Y. Tai, J. Bazin, H. Kim, and I. Kweon, "Partial sum minimization of singular values in robust PCA: Algorithm and applications," *IEEE Transactions on Pattern Analysis and Machine Intelligence*, vol. 38, no. 4, pp. 744–758, 2016.
- [10] L. Wu, A. Ganesh, B. Shi, Y. Matsushita, Y. Wang, and Y. Ma, "Robust photometric stereo via low-rank matrix completion and recovery," in *Proceedings of the 10th Asian Conference on Computer Vision*, 2010, pp. 703–717.
- [11] J. Yang, L. Luo, J. Qian, Y. Tai, F. Zhang, and Y. Xu, "Nuclear norm based matrix regression with applications to face recognition with occlusion and illumination changes," *IEEE Transactions on Pattern Analysis and Machine Intelligence*, vol. 39, no. 1, pp. 156–171, 2017.
- [12] G. Liu, Z. Lin, S. Yan, J. Sun, Y. Yu, and Y. Ma, "Robust recovery of subspace structures by low-rank representation," *IEEE Transactions on Pattern Analysis and Machine Intelligence*, vol. 35, no. 1, pp. 171–184, 2013.
- [13] S. Ji and J. Ye, "An accelerated gradient method for trace norm minimization," in *Proceedings of the 26th International Conference on Machine Learning*, 2009, pp. 457–464.
- [14] R. Mazumder, T. Hastie, and R. Tibshirani, "Spectral regularization algorithms for learning large incomplete matrices," *Journal of Machine Learning Research*, vol. 11, pp. 2287–2322, 2010.
- [15] Q. Yao and J. Kwok, "Accelerated inexact Soft-Impute for fast large-scale matrix completion," in *Proceedings of the 24th International Joint Conference on Artificial Intelligence*, 2015, pp. 4002–4008.
- [16] X. Zhang, D. Schuurmans, and Y.-L. Yu, "Accelerated training for matrix-norm regularization: A boosting approach," in *Advances in Neural Information Processing Systems*, 2012, pp. 2906–2914.
- [17] C.-J. Hsieh and P. Olsen, "Nuclear norm minimization via active subspace selection," in *Proceedings of the 31st International Conference on Machine Learning*, 2014, pp. 575–583.
- [18] T. Zhang, "Analysis of multi-stage convex relaxation for sparse regularization," *Journal of Machine Learning Research*, vol. 11, pp. 1081–1107, 2010.
- [19] E. Candès, M. Wakin, and S. Boyd, "Enhancing sparsity by reweighted ℓ_1 minimization," *Journal of Fourier Analysis and Applications*, vol. 14, no. 5–6, pp. 877–905, 2008.
- [20] J. Fan and R. Li, "Variable selection via nonconcave penalized likelihood and its oracle properties," *Journal of the American Statistical Association*, vol. 96, no. 456, pp. 1348–1360, 2001.
- [21] C. Zhang, "Nearly unbiased variable selection under minimax concave penalty," *Annals of Statistics*, vol. 38, no. 2, pp. 894–942, 2010.
- [22] H. Gui, J. Han, and Q. Gu, "Towards faster rates and oracle property for low-rank matrix estimation," in *Proceedings of the 33rd International Conference on Machine Learning*, 2016, pp. 2300–2309.
- [23] A. Yuille and A. Rangarajan, "The concave-convex procedure," *Neural Computation*, vol. 15, no. 4, pp. 915–936, 2003.
- [24] P. Gong, C. Zhang, Z. Lu, J. Huang, and J. Ye, "A general iterative shrinkage and thresholding algorithm for non-convex regularized optimization problems," in *Proceedings of the 30th International Conference on Machine Learning*, 2013, pp. 37–45.
- [25] H. Li and Z. Lin, "Accelerated proximal gradient methods for non-convex programming," in *Advances in Neural Information Processing Systems*, 2015, pp. 379–387.
- [26] C. Lu, C. Zhu, C. Xu, S. Yan, and Z. Lin, "Generalized singular value thresholding," in *Proceedings of the 29th AAAI Conference on Artificial Intelligence*, 2015, pp. 1805–1811.
- [27] N. Halko, P.-G. Martinsson, and J. Tropp, "Finding structure with randomness: Probabilistic algorithms for constructing approximate matrix decompositions," *SIAM Review*, vol. 53, no. 2, pp. 217–288, 2011.
- [28] Q. Yao, J. Kwok, and W. Zhong, "Fast low-rank matrix learning with nonconvex regularization," in *Proceedings of the 15th International Conference on Data Mining*, 2015, pp. 539–548.
- [29] N. Parikh and S. Boyd, "Proximal algorithms," *Foundations and Trends in Optimization*, vol. 1, no. 3, pp. 127–239, 2014.
- [30] A. Beck and M. Teboulle, "A fast iterative shrinkage-thresholding algorithm for linear inverse problems," *SIAM Journal on Imaging Sciences*, vol. 2, no. 1, pp. 183–202, 2009.
- [31] S. Ghadimi and G. Lan, "Accelerated gradient methods for non-convex nonlinear and stochastic programming," *Mathematical Programming*, vol. 156, no. 1–2, pp. 59–99, 2016.
- [32] J.-F. Cai, E. Candès, and Z. Shen, "A singular value thresholding algorithm for matrix completion," *SIAM Journal on Optimization*, vol. 20, no. 4, pp. 1956–1982, 2010.
- [33] T. Oh, Y. Matsushita, Y. Tai, and I. Kweon, "Fast randomized singular value thresholding for nuclear norm minimization," in *Proceedings of the 28th Conference on Computer Vision and Pattern Recognition*, 2015, pp. 4484–4493.
- [34] K.-C. Toh and S. Yun, "An accelerated proximal gradient algorithm for nuclear norm regularized linear least squares problems," *Pacific Journal of Optimization*, vol. 6, no. 615–640, p. 15, 2010.
- [35] Z. Lin, M. Chen, and Y. Ma, "The augmented Lagrange multiplier method for exact recovery of corrupted low-rank matrices," School of EECS, Peking University, Tech. Rep. arXiv:1009.5055, 2010.
- [36] R. Larsen, "Lanczos bidiagonalization with partial reorthogonalization," Department of Computer Science, Aarhus University, DAIMI PB-357, 1998.
- [37] H. Attouch, J. Bolte, and B. Svaiter, "Convergence of descent methods for semi-algebraic and tame problems: Proximal algorithms, forward-backward splitting, and regularized Gauss-Seidel methods," *Mathematical Programming*, vol. 137, no. 1–2, pp. 91–129, 2013.
- [38] M. Schmidt, N. Roux, and F. Bach, "Convergence rates of inexact proximal-gradient methods for convex optimization," in *Advances in Neural Information Processing Systems*, 2011, pp. 1458–1466.
- [39] J. Hiriart-Urruty, "Generalized differentiability, duality and optimization for problems dealing with differences of convex functions," *Convexity and Duality in Optimization*, pp. 37–70, 1985.
- [40] Y. Nesterov, *Introductory Lectures on Convex Optimization: A Basic Course*. Springer, 2004.
- [41] Z. Wen, W. Yin, and Y. Zhang, "Solving a low-rank factorization model for matrix completion by a nonlinear successive over-relaxation algorithm," *Mathematical Programming Computation*, vol. 4, no. 4, pp. 333–361, 2012.
- [42] Z. Wang, M. Lai, Z. Lu, W. Fan, H. Davulcu, and J. Ye, "Orthogonal rank-one matrix pursuit for low rank matrix completion," *SIAM Journal on Scientific Computing*, vol. 37, no. 1, pp. A488–A514, 2015.
- [43] R. Gemulla, E. Nijkamp, P. Haas, and Y. Sismanis, "Large-scale matrix factorization with distributed stochastic gradient descent," in *Proceedings of the 17th International Conference on Knowledge Discovery and Data Mining*, 2011, pp. 69–77.
- [44] H.-F. Yu, C.-J. Hsieh, S. Si, and I. Dhillon, "Scalable coordinate descent approaches to parallel matrix factorization for recommender systems," in *Proceedings of the 12nd International Conference on Data Mining*, 2012, pp. 765–774.
- [45] B. Recht and C. Ré, "Parallel stochastic gradient algorithms for large-scale matrix completion," *Mathematical Programming Computation*, vol. 5, no. 2, pp. 201–226, 2013.
- [46] J. Demmel, M. Heath, and H. Van Der Vorst, "Parallel numerical linear algebra," *Acta Numerica*, vol. 2, pp. 111–197, 1993.
- [47] H. Avron, S. Kale, V. Sindhwani, and S. Kasiviswanathan, "Efficient and practical stochastic subgradient descent for nuclear norm regularization," in *Proceedings of the 29th International Conference on Machine Learning*, 2012, pp. 1231–1238.
- [48] Y. Zhuang, W.-S. Chin, Y.-C. Juan, and C.-J. Lin, "A fast parallel SGD for matrix factorization in shared memory systems," in *Proceedings of the 7th ACM Conference on Recommender Systems*, 2013, pp. 249–256.
- [49] G. Goumas, K. Kourtis, N. Anastopoulos, V. Karakasis, and N. Koziris, "Understanding the performance of sparse matrix-vector multiplication," in *Proceedings of the 16th Euromicro Conference on Parallel, Distributed and Network-Based Processing*, 2008, pp. 283–292.
- [50] D. Bertsekas and J. Tsitsiklis, *Parallel and Distributed Computation: Numerical Methods*. Athena Scientific, 1997.
- [51] D. Bertsekas, *Nonlinear Programming*. Athena Scientific, 1999.
- [52] C. Rao, "Separation theorems for singular values of matrices and their applications in multivariate analysis," *Journal of Multivariate Analysis*, vol. 9, no. 3, pp. 362–377, 1979.
- [53] P. Arbenz, "Solving large scale eigenvalue problems," Department of Mathematics, ETH Zürich, Lecture Notes, 2010. [Online]. Available: <http://people.inf.ethz.ch/arbenz/ewp/>
- [54] A. Lewis and H. Sendov, "Nonsmooth analysis of singular values," *Set-Valued Analysis*, vol. 13, no. 3, pp. 243–264, 2005.

APPENDIX A

PARALLEL FANCL-ACC

Algorithm 12 shows the parallel version of FaNCL-acc. Acceleration is performed at step 6. The first inexact proximal step is performed at steps 8-18. Step 19 checks whether the accelerated iterate is accepted. If the condition fails, a second inexact proximal step is performed at steps 22-32. Note that the algorithm is equivalent to Algorithm 6, and thus the convergence analysis in Section 3.6 still holds.

Algorithm 12 FaNCL-acc in parallel: FaNCL-acc-PL.

Input: choose $\tau > \rho$, $\lambda_0 > \lambda$, $\delta > 0$ and $\nu \in (0, 1)$;

- 1: initialize $\mathbf{V}_0, \mathbf{V}_1 \in \mathbb{R}^n$ as random Gaussian matrices, $\mathbf{X}_0 = \mathbf{X}_1 = \mathbf{0}$ and $\alpha_0 = \alpha_1 = 1$;
- 2: partition $\mathbf{X}_0, \mathbf{X}_1, \mathcal{P}_\Omega(\mathbf{X}_0), \mathcal{P}_\Omega(\mathbf{X}_1)$ and $\mathcal{P}_\Omega(\mathbf{O})$;
- 3: start q threads for parallelization;
- 4: **for** $t = 1, 2, \dots, T$ **do**
- 5: $\lambda_t = (\lambda_{t-1} - \lambda)\nu^t + \lambda$;
- 6: $\triangleright \mathbf{Y}_t = \mathbf{X}_t + \frac{\alpha_{t-1}-1}{\alpha_t}(\mathbf{X}_t - \mathbf{X}_{t-1})$;
- 7: $\triangleright \mathbf{R}_t = \text{IndeSpan-PL}([\mathbf{V}_t, \mathbf{V}_{t-1}])$;
- 8: $\triangleright \mathbf{A}_t^a = \mathbf{Y}_t - \frac{1}{\tau}\mathcal{P}_\Omega(\mathbf{Y}_t - \mathbf{O})$;
- 9: **for** $p = 1, 2, \dots$ **do**
- 10: $\triangleright [\tilde{\mathbf{X}}_p, \mathbf{R}_t] = \text{ApproxGSVT-PL}(\mathbf{A}_t^a, \mathbf{R}_t, \frac{\lambda}{\tau})$;
- 11: $\triangleright a_p = F(\tilde{\mathbf{X}}_p)$;
- 12: $\triangleright a_t = F(\mathbf{X}_t)$;
- 13: $\triangleright a_F = \|\tilde{\mathbf{X}}_p - \mathbf{X}_t\|_F^2$;
- 14: **if** $a_p \leq a_t - c_1 a_F$ **then**
- 15: **break**;
- 16: **end if**
- 17: **end for**
- 18: $\triangleright \mathbf{X}_{t+1}^a = \tilde{\mathbf{X}}_p$;
- 19: **if** $F(\mathbf{X}_{t+1}^a) \leq F(\mathbf{X}_t) - \frac{\delta}{2}\|\mathbf{X}_{t+1}^a - \mathbf{Y}_t\|_F^2$ **then**
- 20: $\triangleright \mathbf{X}_{t+1} = \mathbf{X}_{t+1}^a$;
- 21: **else**
- 22: $\triangleright \mathbf{A}_t = \mathbf{X}_t - \frac{1}{\tau}\mathcal{P}_\Omega(\mathbf{X}_t - \mathbf{O})$;
- 23: **for** $p = 1, 2, \dots$ **do**
- 24: $\triangleright [\tilde{\mathbf{X}}_p, \mathbf{R}_t] = \text{ApproxGSVT-PL}(\mathbf{A}_t, \mathbf{R}_t, \frac{\lambda}{\tau})$;
- 25: $\triangleright b_p = F(\tilde{\mathbf{X}}_p)$;
- 26: $\triangleright b_t = F(\mathbf{X}_t)$;
- 27: $\triangleright b_F = \|\tilde{\mathbf{X}}_p - \mathbf{X}_t\|_F^2$;
- 28: **if** $b_p \leq b_t - c_1 b_F$ **then**
- 29: **break**;
- 30: **end if**
- 31: **end for**
- 32: $\triangleright \mathbf{X}_{t+1} = \tilde{\mathbf{X}}_p$;
- 33: **end if**
- 34: $\alpha_{t+1} = \frac{1}{2}(\sqrt{4\alpha_t^2 + 1} + 1)$;
- 35: **end for**
- 36: **return** \mathbf{X}_{T+1} .

APPENDIX B

THE CHECKING CONDITION IN [37]

The condition in [37] to accept an approximate $\tilde{\mathbf{X}}_p$ is: $\exists \mathbf{A} \in \partial \tilde{r}(\tilde{\mathbf{X}}_p) - \partial \tilde{r}(\tilde{\mathbf{X}}_p)$ where \tilde{r} and \tilde{r} are two convex functions, such that $\|\mathbf{A} + \nabla f(\tilde{\mathbf{X}}_p)\|_F^2 \leq b\|\tilde{\mathbf{X}}_p - \mathbf{X}\|_F^2$ for some constant $b > 0$. Using the LSP regularizer as an

example. Using Proposition 3.6, we can decompose $r(\tilde{\mathbf{X}}_p)$ as $\tilde{r}(\tilde{\mathbf{X}}_p) + \tilde{r}(\tilde{\mathbf{X}}_p)$, where

$$\begin{aligned}\tilde{r}(\tilde{\mathbf{X}}_p) &= \frac{1}{\theta} \|\tilde{\mathbf{X}}_p\|_*, \\ \tilde{r}(\tilde{\mathbf{X}}_p) &= \sum_{i=1}^n \left[\frac{\sigma_i(\tilde{\mathbf{X}}_p)}{\theta} - \log \left(1 + \frac{\sigma_i(\tilde{\mathbf{X}}_p)}{\theta} \right) \right].\end{aligned}$$

Let the SVD of $\tilde{\mathbf{X}}_p$ be $\mathbf{U}\Sigma\mathbf{V}^\top$. Assume that $\tilde{\mathbf{X}}_p$ has k singular values larger than 0. Let \mathbf{U}_k (resp. \mathbf{V}_k) be the matrix containing the first k columns of \mathbf{U} (resp. \mathbf{V}). Then,

$$\partial \tilde{r}(\tilde{\mathbf{X}}_p) = \frac{1}{\theta} (\mathbf{U}_k \mathbf{V}_k^\top + \mathbf{B}),$$

where $\mathbf{B} \in \{\mathbf{C} : \mathbf{U}_k^\top \mathbf{C} = \mathbf{0}, \mathbf{C} \mathbf{V}_k = \mathbf{0}, \text{ and } \sigma_1(\mathbf{C}) \leq 1\}$. Let $\mathbf{c} = [c_i]$ with $c_i = \frac{1}{\theta} - \frac{1}{\sigma_i(\tilde{\mathbf{X}}_p) + \theta}$. Then,

$$\partial \tilde{r}(\tilde{\mathbf{X}}_p) = \mathbf{U} \text{Diag}(\mathbf{c}) \mathbf{V}^\top.$$

Thus, a full SVD on $\tilde{\mathbf{X}}_p$ is needed, which is expensive and impractical for large matrices.

APPENDIX C

PROOFS

C.1 Proposition 3.1

For simplicity of notations, we write $\sigma_i(\mathbf{Z})$ as σ_i . First, we introduce the definition of super-gradient for a concave function and two lemmas.

Definition 2 ([51]). *For a concave function f , its super-gradient is given by $g \in \hat{\partial} f \equiv \partial(-f)$.*

Lemma C.1 ([51]). *(i) $\inf_{g \in \hat{\partial} \tilde{r}(y)} g \geq 0$; (ii) Assume that $y_j \geq y_i \geq 0$. Then, $\sup_{g_j \in \hat{\partial} \tilde{r}(y_j)} g_j \leq \inf_{g_i \in \hat{\partial} \tilde{r}(y_i)} g_i$.*

Lemma C.2. *(i) $y_i^* - \max(\sigma_i - \mu g_i, 0) = 0$, where $g_i \in \hat{\partial} \tilde{r}(y_i^*)$; (ii) if $y_i^* > 0$, then y_i^* increases with σ_i .*

Proof. (Part (i)): Let $g_i \in \hat{\partial} \tilde{r}(y_i^*)$. From the first-order optimality condition of (4), consider the two possibilities:

- (a) $\sigma_i + \mu g_i \leq 0$: In other words, the optimal solution is achieved at the boundary, and $y_i^* = 0$.
- (b) $\sigma_i + \mu g_i > 0$: We have $0 = y_i^* - \sigma_i + \mu g_i$, and $y_i^* > 0$.

Combining these two cases, the relationship between y_i^* and σ_i can be expressed as

$$y_i^* = \max(\sigma_i - \mu g_i, 0). \quad (12)$$

(Part (ii)): Assume that $y_i^* > 0$. Then, (12) becomes

$$y_i^* = \sigma_i - \mu g_i. \quad (13)$$

Let σ_i becomes larger as σ_j . according to (13), we have two possibilities for its corresponding y_j^* , i.e.,

- $y_j^* > y_i^*$: Then, $\sup_{g_j \in \hat{\partial} \tilde{r}(y_j^*)} g_j \leq \inf_{g_i \in \hat{\partial} \tilde{r}(y_i^*)} g_i$ from Lemma C.1. Together with the fact that $\sigma_j > \sigma_i$, there exists a y_j^* which is not smaller than y_i^* to make (12) hold.
- $y_j^* \leq y_i^*$: Then, $\inf_{g_j \in \hat{\partial} \tilde{r}(y_j^*)} g_j \geq \sup_{g_i \in \hat{\partial} \tilde{r}(y_i^*)} g_i$ from Lemma C.1. However, such a solution may not exist (e.g., when $\hat{r}(\alpha) = \alpha$).

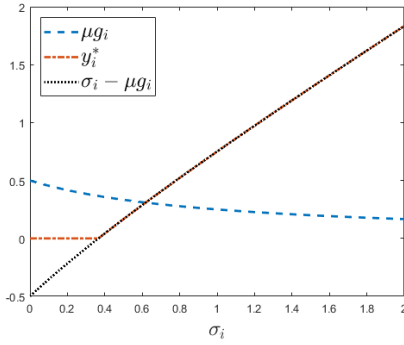
Thus, while there can be multiple solutions to ensure (13), the first case must exist. We take the largest solution of all possible candidates. Thus, if σ_i gets larger, y_i^* also becomes larger.

□

Proof of Proposition 3.1. From Lemma C.2, we have

$$0 = y_i^* - \max(\sigma_i - \mu g_i, 0).$$

We can see that $y^* = 0$ once $\sigma_i - \mu g_i \leq 0$. However, if σ_i becomes smaller, $\sigma_i - \mu g_i$ will reach 0 before σ_i reaches zero. This comes from two facts. First, y_i^* becomes smaller as σ_i gets smaller (Lemma C.2), but $\inf_{g_i \in \partial \hat{r}(y_i^*)} g_i$ will not become smaller (Lemma C.1). Second, we have $\lim_{y \rightarrow 0^+} \inf_{g \in \partial \hat{r}(y)} g > 0$. An illustration of the relationships among σ_i , y_i^* and g_i is shown in the following figure. Thus, there exists $\gamma > 0$ such that once $\sigma_i \leq \gamma$, $\sigma_i - \mu g_i \leq 0$, and y_i^* becomes 0.



C.2 Corollary 3.2

In this section, we show how to derive the threshold γ for the capped- ℓ_1 penalty. Derivations for the other penalties can be obtained similarly.

C.2.1 Capped- ℓ_1 Penalty

Proof. Note that problem (4) considers each singular value separately. For simplicity of notations, let σ_i denote $\sigma_i(\mathbf{Z})$. For the i th singular value, let

$$h(y_i) \equiv \frac{1}{2}(y_i - \sigma_i)^2 + \mu \min(y_i, \theta).$$

Thus,

$$\arg \min_{y_i \geq 0} h(y_i) = \begin{cases} \arg \min_{0 \leq y_i \leq \theta} h_1(y_i) \\ \arg \min_{y_i > \theta} h_2(y_i) \end{cases},$$

where

$$\begin{aligned} h_1(p_i) &= \frac{1}{2}(p_i - \sigma_i)^2 + \mu p_i, \\ h_2(q_i) &= \frac{1}{2}(q_i - \sigma_i)^2 + \mu \theta. \end{aligned}$$

Note that h_1 is quadratic. There are only three possibilities for $p_i^* = \arg \min_{0 \leq p_i \leq \theta} h_1(p_i)$, i.e.,

$$\min_{0 \leq p_i \leq \theta} h_1(p_i) = \begin{cases} \frac{1}{2}\sigma_i^2 & \text{if } p_i^* = 0 \\ \mu\sigma_i - \frac{1}{2}\mu^2 & \text{if } p_i^* = \sigma_i - \mu \\ \frac{1}{2}(\theta - \sigma_i)^2 + \mu\sigma_i & \text{if } p_i^* = \theta \end{cases},$$

and

$$p_i^* = \begin{cases} 0 & \text{if } 0 \leq \sigma_i \leq \mu \\ \sigma_i - \mu & \text{if } \mu < \sigma_i \leq \mu + \theta \\ \theta & \text{otherwise} \end{cases}. \quad (14)$$

Let $q_i^* = \arg \min_{q_i > \theta} h_2(q_i)$. As h_2 is also quadratic and q_i^* cannot be θ , we have

$$q_i^* = \begin{cases} \text{no solution} & \text{if } 0 \leq \sigma_i \leq \theta \\ \sigma_i & \text{otherwise} \end{cases}. \quad (15)$$

Note that when $\sigma_i \in [0, \theta]$, there is no solution to q_i^* , as q_i^* can arbitrarily close to θ . Since $h_1(\theta) = h_2(\theta)$, the possibility for $\theta = \arg \min_{y_i \geq 0} h(y_i)$ is covered by $\arg \min_{0 \leq p_i \leq \theta} h_1$. Thus, (14) and (15) have covered all possibilities of y_i^* . Using them, we have

1) If $\theta \leq \mu$, then

$$\min_{y_i \geq 0} h = \begin{cases} h_1(0) & 0 \leq \sigma_i \leq \theta \\ \min(h_1(0), h_2(\sigma_i)) & \theta < \sigma_i \leq \mu \\ \min(h_1(\sigma_i - \mu), h_2(\sigma_i)) & \mu < \sigma_i \leq \mu + \theta \\ \min(h_1(\theta), h_2(\sigma_i)) & \sigma_i > \mu + \theta \end{cases}.$$

In order to get $y_i^* = 0$, we need

$$\min(h_1(0), h_2(\sigma_i)) = h_1(0),$$

which leads to

$$\sigma_i \leq \sqrt{2\mu\theta}.$$

Thus, if $0 \leq \sigma_i \leq \min(\sqrt{2\mu\theta}, \mu)$, then $y_i^* = 0$.

2) If $\theta > \mu$, then

$$\min_{y_i \geq 0} h = \begin{cases} h_1(0) & 0 \leq \sigma_i \leq \mu \\ h_1(\sigma_i - \mu) & \mu < \sigma_i \leq \theta \\ \min(h_1(\sigma_i - \mu), h_2(\sigma_i)) & \theta < \sigma_i \leq \mu + \theta \\ \min(h_1(\theta), h_2(\sigma_i)) & \sigma_i > \mu + \theta \end{cases}.$$

Thus, if $0 \leq \sigma_i \leq \mu$, then we have $y_i^* = 0$.

Finally, combining the above two cases, we can conclude that once $\sigma_i \leq \min(\sqrt{2\mu\theta}, \mu)$, then $y_i^* = 0$. Thus, $\gamma = \min(\sqrt{2\mu\theta}, \mu)$. □

C.3 Proposition 3.3

Proof. First, we introduce the following theorem.

Theorem C.3 (Separation theorem [52]). Let $\mathbf{A} \in \mathbb{R}^{m \times n}$ and $\mathbf{B} \in \mathbb{R}^{m \times r}$ with $\mathbf{B}^\top \mathbf{B} = \mathbf{I}$. Then

$$\sigma_i(\mathbf{B}^\top \mathbf{A}) \leq \sigma_i(\mathbf{A}), \text{ for } i = 1, \dots, \min(r, n).$$

Let the SVD of \mathbf{Z} be $\mathbf{U}\Sigma\mathbf{V}^\top$. \mathbf{Z} can then be rewritten as

$$\mathbf{Z} = [\mathbf{U}_{\hat{k}}; \mathbf{U}_\perp] \begin{bmatrix} \Sigma_{\hat{k}} & \\ & \Sigma_\perp \end{bmatrix} [\mathbf{V}_{\hat{k}}; \mathbf{V}_\perp]^\top, \quad (16)$$

where $\mathbf{U}_{\hat{k}}$ contains the \hat{k} leading columns of \mathbf{U} , and \mathbf{U}_\perp the remaining columns. Similarly, $\Sigma_{\hat{k}}$ (resp. $\mathbf{V}_{\hat{k}}$) contains the \hat{k} leading eigenvalues (resp. columns) of Σ (resp. \mathbf{V}). Hence,

$$\sigma_i(\mathbf{Q}^\top \mathbf{Z}) = \max_{\tilde{\mathbf{u}}_i, \tilde{\mathbf{v}}_i} \tilde{\mathbf{u}}_i^\top (\mathbf{Q}^\top \mathbf{Z}) \tilde{\mathbf{v}}_i. \quad (17)$$

Let

$$\tilde{\mathbf{u}}_i = \mathbf{Q}^\top \mathbf{u}_i \quad \text{and} \quad \tilde{\mathbf{v}}_i = \mathbf{v}_i, \quad (18)$$

where \mathbf{u}_i (resp. \mathbf{v}_i) is the i th column of \mathbf{U} (resp. \mathbf{V}).

$$\begin{aligned} \tilde{\mathbf{u}}_i^\top (\mathbf{Q}^\top \mathbf{Z}) \tilde{\mathbf{v}}_i &= \mathbf{u}_i^\top (\mathbf{Q} \mathbf{Q}^\top) \mathbf{Z} \mathbf{v}_i \\ &= \mathbf{u}_i^\top \mathbf{Z} \mathbf{v}_i \\ &= \sigma_i(\mathbf{Z}), \end{aligned} \quad (19)$$

$$= \sigma_i(\mathbf{Z}), \quad (20)$$

where (19) is due to $\text{span}(\mathbf{U}_{\hat{k}}) \subseteq \text{span}(\mathbf{Q})$. From Theorem C.3, by substituting $\mathbf{Q} = \mathbf{B}$ and $\mathbf{A} = \mathbf{Z}$, we have $\sigma_i(\mathbf{Q}^\top \mathbf{Z}) \leq \sigma_i(\mathbf{Z})$. Combining with (20), we obtain that (18) is the optimal solution of (17). Thus, the rank- \hat{k} SVD of $\mathbf{Q}^\top \mathbf{Z}$ is $(\mathbf{Q}^\top \mathbf{U}_{\hat{k}}) \Sigma_{\hat{k}} \mathbf{V}_{\hat{k}}^\top$, with the corresponding left and right singular vectors contained in $\mathbf{Q}^\top \mathbf{U}_{\hat{k}}$ and $\mathbf{V}_{\hat{k}}$, respectively.

Again, by Theorem C.3, we have

$$\sigma_{\hat{k}+1}(\mathbf{Q}^\top \mathbf{Z}) \leq \sigma_{\hat{k}+1}(\mathbf{Z}) \leq \gamma.$$

Besides, using (16),

$$\sigma_i(\mathbf{Q}^\top \mathbf{Z}) = \max_{\tilde{\mathbf{u}}, \tilde{\mathbf{v}}} \tilde{\mathbf{u}}^\top (\mathbf{Q}^\top \mathbf{U}_{\hat{k}} \Sigma_{\hat{k}} \mathbf{V}_{\hat{k}}^\top + \mathbf{Q}^\top \mathbf{U}_\perp \Sigma_\perp \mathbf{V}_\perp^\top) \tilde{\mathbf{v}}.$$

The first \hat{k} singular values are from the term $\mathbf{Q}^\top \mathbf{U}_{\hat{k}} \Sigma_{\hat{k}} \mathbf{V}_{\hat{k}}^\top$. Hence,

$$\sigma_{\hat{k}+1}(\mathbf{Q}^\top \mathbf{Z}) = \max_{\tilde{\mathbf{u}}, \tilde{\mathbf{v}}} \tilde{\mathbf{u}}^\top (\mathbf{Q}^\top \mathbf{U}_\perp \Sigma_\perp \mathbf{V}_\perp^\top) \tilde{\mathbf{v}} \leq \gamma. \quad (21)$$

Then,

$$\begin{aligned} \text{prox}_{\mu r}(\mathbf{Q}^\top \mathbf{Z}) &= \text{prox}_{\mu r}(\mathbf{Q}^\top \mathbf{U}_{\hat{k}} \Sigma_{\hat{k}} \mathbf{V}_{\hat{k}}^\top + \mathbf{Q}^\top \mathbf{U}_\perp \Sigma_\perp \mathbf{V}_\perp^\top) \\ &= \text{prox}_{\mu r}(\mathbf{Q}^\top \mathbf{U}_{\hat{k}} \Sigma_{\hat{k}} \mathbf{V}_{\hat{k}}^\top) + \text{prox}_{\mu r}(\mathbf{Q}^\top \mathbf{U}_\perp \Sigma_\perp \mathbf{V}_\perp^\top) \\ &= \text{prox}_{\mu r}(\mathbf{Q}^\top \mathbf{U}_{\hat{k}} \Sigma_{\hat{k}} \mathbf{V}_{\hat{k}}^\top). \end{aligned} \quad (22)$$

$$= \text{prox}_{\mu r}(\mathbf{Q}^\top \mathbf{U}_{\hat{k}} \Sigma_{\hat{k}} \mathbf{V}_{\hat{k}}^\top). \quad (23)$$

where (22) follows from that $\mathbf{Q}^\top \mathbf{U}_{\hat{k}}$ (resp. $\mathbf{V}_{\hat{k}}$) is orthogonal to $\mathbf{Q}^\top \mathbf{U}_\perp$ (resp. \mathbf{V}_\perp). (21) shows that there are only \hat{k} singular values in $\mathbf{Q}^\top \mathbf{Z}$ larger than γ . Thus, $\text{prox}_{\mu r}(\mathbf{Q}^\top \mathbf{U}_\perp \Sigma_\perp \mathbf{V}_\perp^\top) = 0$ and we get (23). Finally,

$$\begin{aligned} \mathbf{Q} \text{prox}_{\mu r}(\mathbf{Q}^\top \mathbf{Z}) &= \mathbf{Q} (\mathbf{Q}^\top \mathbf{U}_{\hat{k}} \text{prox}_{\mu r}(\Sigma_{\hat{k}}) \mathbf{V}_{\hat{k}}^\top) \\ &= \mathbf{U}_{\hat{k}} \text{prox}_{\mu r}(\Sigma_{\hat{k}}) \mathbf{V}_{\hat{k}}^\top \\ &= \text{prox}_{\mu r}(\mathbf{Z}), \end{aligned} \quad (24)$$

$$= \text{prox}_{\mu r}(\mathbf{Z}), \quad (25)$$

where (24) comes from $\text{span}(\mathbf{U}_{\hat{k}}) \subseteq \text{span}(\mathbf{Q})$; (25) comes from that rank- \hat{k} SVD of \mathbf{Z} is $\mathbf{U}_{\hat{k}} \Sigma_{\hat{k}} \mathbf{V}_{\hat{k}}^\top$ and \mathbf{Z} only has \hat{k} singular values larger than γ . \square

C.4 Proposition 3.5

Proof. First, we introduce the following Lemmas.

Lemma C.4 ([27], [53]). *In Algorithm 2, let the SVD of \mathbf{Z} be $\tilde{\mathbf{U}} \tilde{\Sigma} \tilde{\mathbf{V}}^\top$, and $\tilde{\mathbf{U}}_k$ contain the first k columns of $\tilde{\mathbf{U}}$. We have*

$$\|\mathbf{Q}_j \mathbf{Q}_j^\top - \tilde{\mathbf{U}}_k \tilde{\mathbf{U}}_k^\top\|_F \leq \alpha^{j-1} \|\mathbf{C} \mathbf{C}^\top - \tilde{\mathbf{U}}_k \tilde{\mathbf{U}}_k^\top\|_F,$$

where $\alpha = \sigma_{k+1}(\mathbf{Z})/\sigma_k(\mathbf{Z}) \in (0, 1)$ and $\mathbf{C} = \mathbf{Q} \mathbf{R}(\mathbf{Z} \mathbf{R})$.

Lemma C.5. *In Algorithm 4, let the rank- k SVD of \mathbf{A} be $\mathbf{U}_k \Sigma_k \mathbf{V}_k^\top$, and*

$$\mathbf{B}_p = \mathbf{Q} \mathbf{R}(\mathbf{A} \tilde{\mathbf{V}}_p). \quad (26)$$

Then, $\|\mathbf{B}_p \mathbf{B}_p^\top - \mathbf{U}_k \mathbf{U}_k^\top\|_F \leq \eta^p \|\mathbf{B}_0 \mathbf{B}_0^\top - \mathbf{U}_k \mathbf{U}_k^\top\|_F$, where $\eta \in (0, 1)$ is a constant.

Proof. At the p th iteration of Algorithm 4, inside Algorithm 2 (step 3), since $\mathbf{Z} = \mathbf{A}$ and $\mathbf{R} = \tilde{\mathbf{V}}_{p-1}$, we have

$$\mathbf{Q}_1 = \mathbf{Q} \mathbf{R}(\mathbf{A} \tilde{\mathbf{V}}_{p-1}) = \mathbf{B}_{p-1}. \quad (27)$$

Then, for $\tilde{\mathbf{V}}_p$, inside Algorithm 3 (step 2), we have

$$\text{span}(\tilde{\mathbf{V}}_p) = \text{span}(\mathbf{A}^\top \mathbf{Q}).$$

Thus,

$$\begin{aligned} \text{span}(\mathbf{A} \tilde{\mathbf{V}}_p) &= \text{span}(\mathbf{A} (\mathbf{A}^\top \mathbf{Q})) \\ &= \text{span}(\mathbf{A} (\mathbf{A}^\top \mathbf{Q}_J)) \\ &= \text{span}(\mathbf{Y}_{J+1}), \end{aligned} \quad (28)$$

$$= \text{span}(\mathbf{Y}_{J+1}), \quad (29)$$

where (28) comes from the fact that \mathbf{Q} is returned after J iterations of Algorithm 2; and (29) from the definition of \mathbf{Y}_{J+1} at step 4 in Algorithm 2. Thus,

$$\begin{aligned} \mathbf{Q}_{J+1} &= \mathbf{Q} \mathbf{R}(\mathbf{Y}_{J+1}) \\ &= \mathbf{Q} \mathbf{R}(\mathbf{A} \tilde{\mathbf{V}}_p) = \mathbf{B}_p. \end{aligned} \quad (30)$$

Note that $\mathbf{C} = \mathbf{Q}_1$ in Lemma C.4. Together with (27) and (30), we have

$$\begin{aligned} \|\mathbf{B}_p \mathbf{B}_p^\top - \mathbf{U}_k \mathbf{U}_k^\top\|_F &= \|\mathbf{Q}_{J+1} \mathbf{Q}_{J+1}^\top - \mathbf{U}_k \mathbf{U}_k^\top\|_F \\ &\leq \alpha^J \|\mathbf{Q}_1 \mathbf{Q}_1^\top - \mathbf{U}_k \mathbf{U}_k^\top\|_F \\ &= \eta \|\mathbf{B}_{p-1} \mathbf{B}_{p-1}^\top - \mathbf{U}_k \mathbf{U}_k^\top\|_F, \end{aligned}$$

where $\eta = \alpha^J \in (0, 1)$. Thus,

$$\|\mathbf{B}_p \mathbf{B}_p^\top - \mathbf{U}_k \mathbf{U}_k^\top\|_F \leq \eta^p \|\mathbf{B}_0 \mathbf{B}_0^\top - \mathbf{U}_k \mathbf{U}_k^\top\|_F. \quad \square$$

(Proof of Proposition 3.5) For \mathbf{B}_p in (26), we have $\lim_{p \rightarrow \infty} \mathbf{B}_p = \mathbf{U}_k$ from Proposition C.5 where \mathbf{U}_k comes from rank- k SVD of \mathbf{A} . As $k \geq \hat{k}_A$, $\text{span}(\mathbf{U}_{\hat{k}_A}) \subseteq \text{span}(\mathbf{U}_k)$. Then, from Proposition 3.3, we have

$$\mathbf{U}_k \text{prox}_{\frac{\lambda}{r}}(\mathbf{U}_k^\top \mathbf{A}) = \text{prox}_{\frac{\lambda}{r}}(\mathbf{A}).$$

Thus, $\lim_{p \rightarrow \infty} \tilde{\mathbf{X}}_p = \text{prox}_{\frac{\lambda}{r}}(\mathbf{A})$. \square

C.5 Proposition 3.6

Proof. First, we introduce Lemma C.6.

Lemma C.6 ([54]). *Let $\phi(\mathbf{X}) = \sum_{i=1}^m f(\sigma_i(\mathbf{X}))$. If f is convex, ϕ is also convex on \mathbf{X} .*

For \hat{r} in Assumption A3, it can be rewritten as $\hat{r}(\alpha) = \hat{r}_1(\alpha) - \hat{r}_2(\alpha)$, where $\hat{r}_1(\alpha) = \kappa \alpha$ (for some constant κ) and $\hat{r}_2(\alpha) = \kappa \alpha - \hat{r}(\alpha)$. Obviously, both \hat{r}_1 and \hat{r}_2 are convex. Define

$$\check{r}(\mathbf{X}) = \sum_{i=1}^m \hat{r}_1(\sigma_i(\mathbf{X})), \quad \text{and} \quad \tilde{r}(\mathbf{X}) = \sum_{i=1}^m \hat{r}_2(\sigma_i(\mathbf{X})).$$

From Lemma C.6, both \check{r} and \tilde{r} are convex. Thus, r can also be written as a difference of convex functions: $r(\mathbf{X}) = \check{r}(\mathbf{X}) - \tilde{r}(\mathbf{X})$. \square

C.6 Proposition 3.7

Proof. From step 5 of Algorithm 5 (which ensures (5)), we have

$$F(\mathbf{X}_{t+1}) \leq F(\mathbf{X}_t) - c_1 \|\mathbf{X}_{t+1} - \mathbf{X}_t\|_F^2.$$

Summing this from $t = 1$ to T , we have

$$\begin{aligned} c_1 \sum_{t=1}^T \|\mathbf{X}_{t+1} - \mathbf{X}_t\|_F^2 &\leq F(\mathbf{X}_1) - F(\mathbf{X}_{T+1}) \\ &\leq F(\mathbf{X}_1) - \inf F. \end{aligned} \quad (31)$$

As F is bounded from below (Assumption A2),

$$a_1 \equiv F(\mathbf{X}_1) - \inf F$$

is a positive constant. Let $T \rightarrow \infty$, we have

$$\sum_{t=1}^{\infty} \|\mathbf{X}_{t+1} - \mathbf{X}_t\|_F^2 \leq \frac{a_1}{c_1}. \quad (32)$$

From Assumption A2, we also have

$$\lim_{\|\mathbf{X}\|_F \rightarrow \infty} f(\mathbf{X}) \rightarrow \infty,$$

which implies that $\max_{t=1, \dots, \infty} \|\mathbf{X}_t\|_t < \infty$. Together with (32), $\{\mathbf{X}_t\}$ is a bounded sequence with at least one limit point [51]. \square

C.7 Corollary 3.8

Proof. Combining (31) and (32), we have

$$\begin{aligned} \min_{t=1, \dots, T} \|\mathbf{X}_{t+1} - \mathbf{X}_t\|_F^2 &\leq \frac{1}{T} \sum_{t=1}^T \|\mathbf{X}_{t+1} - \mathbf{X}_t\|_F^2 \\ &\leq \frac{1}{T} \sum_{t=1}^{\infty} \|\mathbf{X}_{t+1} - \mathbf{X}_t\|_F^2 \\ &\leq \frac{F(\mathbf{X}_1) - \inf F}{c_1 T}. \end{aligned}$$

\square

C.8 Theorem 3.9

Proof. First, we introduce Lemma C.7.

Lemma C.7 ([24], [37]). *If $\mathbf{X} = \text{prox}_{\frac{\lambda}{\tau} r}(\mathbf{X} - \frac{1}{\tau} \nabla f(\mathbf{X}))$, then \mathbf{X} is a critical point of (1).*

As $\{\mathbf{X}_{t_j}\}$ is a subsequence of $\{\mathbf{X}_t\}$ with limit point \mathbf{X}_* ,

$$\lim_{t_j \rightarrow \infty} \mathbf{X}_{t_j+1} = \text{InexactPS} \left(\lim_{t_j \rightarrow \infty} \mathbf{X}_{t_j}, \lim_{t_j \rightarrow \infty} \mathbf{R}_{t_j} \right), \quad (33)$$

From (32), we have

$$\lim_{t \rightarrow \infty} \|\mathbf{X}_{t+1} - \mathbf{X}_t\|_F^2 = 0,$$

which implies

$$\lim_{t_j \rightarrow \infty} \mathbf{X}_{t_j+1} = \lim_{t_j \rightarrow \infty} \mathbf{X}_{t_j} = \mathbf{X}_*, \quad (34)$$

for $\{\mathbf{X}_{t_j}\}$. Combining (33) and (34), we have

$$\begin{aligned} \lim_{t_j \rightarrow \infty} \mathbf{X}_* &= \text{InexactPS} \left(\lim_{t_j \rightarrow \infty} \mathbf{X}_{t_j}, \lim_{t_j \rightarrow \infty} \mathbf{R}_{t_j} \right), \\ &= \text{InexactPS} \left(\mathbf{X}_*, \lim_{t_j \rightarrow \infty} \mathbf{R}_{t_j} \right). \end{aligned}$$

Thus, $\mathbf{X}_* = \text{prox}_{\frac{\lambda}{\tau} r}(\mathbf{X}_* - \frac{1}{\tau} \nabla f(\mathbf{X}_*))$ holds by the assumption. From Lemma C.7, \mathbf{X}_* is a critical point of (1). \square

C.9 Proposition 3.10

Proof. Consider the two cases:

- 1) Step 8 in Algorithm 6 is performed: Then,

$$F(\mathbf{X}_{t+1}) \leq F(\mathbf{X}_t) - \frac{\delta}{2} \|\mathbf{X}_{t+1} - \mathbf{Y}_t\|_F^2. \quad (35)$$

- 2) Step 10 is performed: Then,

$$F(\mathbf{X}_{t+1}) \leq F(\mathbf{X}_t) - c_1 \|\mathbf{X}_{t+1} - \mathbf{X}_t\|_F^2. \quad (36)$$

Partition the iterations $\{1, \dots, T\}$ into two sets Ω_T^1 and Ω_T^2 , such that $t \in \Omega_T^1$ if step 8 is performed, and $t \in \Omega_T^2$ if step 10 is performed. Sum (35) and (36) from $t = 1$ to T ,

$$\begin{aligned} F(\mathbf{X}_1) - F(\mathbf{X}_{T+1}) &\geq \sum_{t \in \Omega_T^1} \frac{\delta}{2} \|\mathbf{X}_{t+1} - \mathbf{Y}_t\|_F^2 + \sum_{t \in \Omega_T^2} c_1 \|\mathbf{X}_{t+1} - \mathbf{X}_t\|_F^2. \end{aligned} \quad (37)$$

As F is bounded from below (Assumption A2),

$$\sum_{t \in \Omega_\infty^1} \frac{\delta}{2} \|\mathbf{X}_{t+1} - \mathbf{Y}_t\|_F^2 + \sum_{t \in \Omega_\infty^2} c_1 \|\mathbf{X}_{t+1} - \mathbf{X}_t\|_F^2 \leq a_1. \quad (38)$$

where $a_1 = F(\mathbf{X}_1) - \inf F > 0$ is a constant. Consider the three cases:

- 1) $|\Omega_\infty^1|$ is finite but $|\Omega_\infty^2|$ is infinite: For $t_j \in \Omega_\infty^2$, we have from (38)

$$\sum_{t_j \in \Omega_\infty^2} \|\mathbf{X}_{t_j+1} - \mathbf{X}_{t_j}\|_F^2 \leq \frac{a_1}{c_1}. \quad (39)$$

From Assumption A2, we also have

$$\lim_{\|\mathbf{X}\|_F \rightarrow \infty} f(\mathbf{X}) = \infty, \quad (40)$$

which indicates that $\max_{t_j=1, \dots, \infty} \|\mathbf{X}_{t_j}\|_F < \infty$. Together with (39), the sequence $\{\mathbf{X}_t\}$ is bounded, which has at least one limit point [51].

- 2) $|\Omega_\infty^1|$ is infinite but $|\Omega_\infty^2|$ is finite: For $t_j \in \Omega_\infty^1$, note that, $F(\mathbf{X}_{t_j+1}) \leq F(\mathbf{X}_{t_j})$ due to (35) and (36). From Assumption A2,

$$\inf_{\mathbf{X}} F(\mathbf{X}) > -\infty,$$

then the sequence $\{F(\mathbf{X}_{t_j})\}$ is bounded. Again, from Assumption A2, we have (40), then $\{\mathbf{X}_{t_j}\}$ is also bounded which has at least one limit point [51].

- 3) Both $|\Omega_\infty^1|$ and $|\Omega_\infty^2|$ are infinite: As in the above two cases, $\{\mathbf{X}_t\}$ is bounded when either of $|\Omega_\infty^1|$ and $|\Omega_\infty^2|$ is infinite.

Combining the above, $\{\mathbf{X}_t\}$ generated from Algorithm 6 is bounded and has at least one limit point. \square

C.10 Corollary 3.11

Proof. Let $c_2 = \min(\delta/2, c_1)$. From (37), we have

$$\begin{aligned} F(\mathbf{X}_1) - F(\mathbf{X}_{T+1}) &\geq c_2 \left(\sum_{t \in \Omega_T^1} \|\mathbf{X}_{t+1} - \mathbf{Y}_t\|_F^2 + \sum_{t \in \Omega_T^2} \|\mathbf{X}_{t+1} - \mathbf{X}_t\|_F^2 \right) \\ &= c_2 \sum_{t=1}^T \|\mathbf{X}_{t+1} - \mathbf{C}_t\|_F^2. \end{aligned} \quad (41)$$

Thus,

$$\begin{aligned} \min_{t=1,\dots,T} \|\mathbf{X}_{t+1} - \mathbf{C}_t\|_F^2 &\leq \frac{1}{T} \sum_{t=1}^T \|\mathbf{X}_{t+1} - \mathbf{C}_t\|_F^2 \\ &\leq \frac{1}{T} \sum_{t=1}^{\infty} \|\mathbf{X}_{t+1} - \mathbf{C}_t\|_F^2 \\ &\leq \frac{F(\mathbf{X}_1) - \inf F}{c_2 T}, \end{aligned}$$

where the last inequality comes from (41). \square

C.11 Theorem 3.12

Proof. Partition the iterations $\{1, \dots, \infty\}$ into two sets Ω_{∞}^1 and Ω_{∞}^2 , such that $t \in \Omega_{\infty}^1$ if step 8 is performed, and $t \in \Omega_{\infty}^2$ if step 10 is performed. Consider the three cases:

- 1) $|\Omega_{\infty}^1|$ is finite but $|\Omega_{\infty}^2|$ is infinite: Let $\{\mathbf{X}_{t_j}\}$ be a subsequence of $\{\mathbf{X}_t\}$ where $t \in \Omega_{\infty}^2$, and $\lim_{t_j \rightarrow \infty} \mathbf{X}_{t_j} = \mathbf{X}_*$. From (39), we have

$$\lim_{t_j \rightarrow \infty} \mathbf{X}_{t_j} = \lim_{t_j \rightarrow \infty} \mathbf{X}_{t_j+1} = \mathbf{X}_*. \quad (42)$$

Besides,

$$\lim_{t_j \rightarrow \infty} \mathbf{X}_{t_j+1} = \text{InexactPS} \left(\lim_{t_j \rightarrow \infty} \mathbf{X}_{t_j}, \lim_{t_j \rightarrow \infty} \mathbf{R}_{t_j} \right). \quad (43)$$

Combining (42) and (43), we have

$$\begin{aligned} \lim_{t_j \rightarrow \infty} \mathbf{X}_{t_j+1} &= \text{InexactPS} \left(\lim_{t_j \rightarrow \infty} \mathbf{X}_{t_j}, \lim_{t_j \rightarrow \infty} \mathbf{R}_{t_j} \right) \\ &= \text{InexactPS} \left(\mathbf{X}_*, \lim_{t_j \rightarrow \infty} \mathbf{R}_{t_j} \right) \\ &= \mathbf{X}_*. \end{aligned}$$

Thus, by the assumption, we also have

$$\mathbf{X}_* = \text{prox}_{\frac{\Delta}{\tau}}(\mathbf{X}_* - \frac{1}{\tau} \nabla f(\mathbf{X}_*)).$$

From Lemma C.7, \mathbf{X}_* is also a critical point of (1).

- 2) $|\Omega_{\infty}^1|$ is infinite but $|\Omega_{\infty}^2|$ is finite: Let $\{\mathbf{X}_{t_j}\}$ be a subsequence of $\{\mathbf{X}_t\}$ where $t \in \Omega_{\infty}^1$, and $\lim_{t_j \rightarrow \infty} \mathbf{X}_{t_j} = \mathbf{X}_*$. From (37), we have

$$\sum_{t \in \Omega_{\infty}^1} \frac{\delta}{2} \|\mathbf{X}_{t+1} - \mathbf{Y}_t\|_F^2 < \infty$$

which indicates

$$\lim_{t_j \rightarrow \infty} \mathbf{X}_{t_j+1} - \mathbf{Y}_{t_j} = 0. \quad (44)$$

From (44), we have

$$\lim_{t_j \rightarrow \infty} \mathbf{Y}_{t_j} = \lim_{t_j \rightarrow \infty} \mathbf{X}_{t_j+1} = \mathbf{X}_*. \quad (45)$$

Besides,

$$\lim_{t_j \rightarrow \infty} \mathbf{X}_{t_j+1} = \text{InexactPS} \left(\lim_{t_j \rightarrow \infty} \mathbf{Y}_{t_j}, \lim_{t_j \rightarrow \infty} \mathbf{R}_{t_j} \right). \quad (46)$$

Combining (45) and (46), we have

$$\begin{aligned} \lim_{t_j \rightarrow \infty} \mathbf{X}_{t_j+1} &= \text{InexactPS} \left(\lim_{t_j \rightarrow \infty} \mathbf{Y}_{t_j}, \lim_{t_j \rightarrow \infty} \mathbf{R}_{t_j} \right) \\ &= \text{InexactPS} \left(\mathbf{X}_*, \lim_{t_j \rightarrow \infty} \mathbf{R}_{t_j} \right) \\ &= \mathbf{X}_*. \end{aligned}$$

Thus, by the assumption, we also have

$$\mathbf{X}_* = \text{prox}_{\frac{\Delta}{\tau}}(\mathbf{X}_* - \frac{1}{\tau} \nabla f(\mathbf{X}_*)).$$

From Lemma C.7, \mathbf{X}_* is also a critical point of (1).

- 3) Both $|\Omega_{\infty}^1|$ and $|\Omega_{\infty}^2|$ are infinite: From the above two cases, we can see that the limit point \mathbf{X}_* is also a critical point of (1) when either $|\Omega_{\infty}^1|$ or $|\Omega_{\infty}^2|$ is infinite.

Thus, limit points of $\{\mathbf{X}_t\}$ are also critical points of (1). \square

C.12 Proposition 4.1

Proof. Consider the two cases:

- 1) Steps 10 and 11 are performed: Then,

$$\begin{aligned} F(\mathbf{X}_{t+1}, \mathbf{S}_{t+1}) &\leq F(\mathbf{X}_t, \mathbf{S}_t) \\ &\quad - \frac{\delta}{2} (\|\mathbf{X}_{t+1} - \mathbf{Y}_t^{\mathbf{X}}\|_F^2 + \|\mathbf{S}_{t+1} - \mathbf{Y}_t^{\mathbf{S}}\|_F^2). \end{aligned} \quad (47)$$

- 2) Steps 13 and 14 are performed: Then,

$$\begin{aligned} F(\mathbf{X}_{t+1}, \mathbf{S}_{t+1}) &\leq F(\mathbf{X}_t, \mathbf{S}_t) \\ &\quad - (c_1 \|\mathbf{X}_{t+1} - \mathbf{X}_t\|_F^2 + \frac{\tau - \rho}{2} \|\mathbf{S}_{t+1} - \mathbf{S}_t\|_F^2). \end{aligned} \quad (48)$$

Partition $\{1, \dots, T\}$ into two sets as Ω_T^1 and Ω_T^2 , where $t \in \Omega_T^1$ if steps 10-11 are performed; otherwise, $t \in \Omega_T^2$ (and steps 13-14 are performed). Let

$$\begin{aligned} \Theta_T &= \sum_{t \in \Omega_T^1} \frac{\delta}{2} (\|\mathbf{X}_{t+1} - \mathbf{Y}_t^{\mathbf{X}}\|_F^2 + \|\mathbf{S}_{t+1} - \mathbf{Y}_t^{\mathbf{S}}\|_F^2) \\ &\quad + \sum_{t \in \Omega_T^2} (c_1 \|\mathbf{X}_{t+1} - \mathbf{X}_t\|_F^2 + \frac{\tau - \rho}{2} \|\mathbf{S}_{t+1} - \mathbf{S}_t\|_F^2). \end{aligned}$$

Summing (47) and (48) from $t = 1$ to T , we have

$$F(\mathbf{X}_1, \mathbf{S}_1) - F(\mathbf{X}_{T+1}, \mathbf{S}_{T+1}) \geq \Theta_T. \quad (49)$$

As F is bounded from below (Assumption A2), we have

$$\Theta_{\infty} \leq a_2, \quad (50)$$

where $a_2 = F(\mathbf{X}_1, \mathbf{S}_1) - \inf F$. We consider the three cases:

- 1) $|\Omega_{\infty}^1|$ is finite but $|\Omega_{\infty}^2|$ is infinite: For $t_j \in \Omega_{\infty}^2$,

$$\begin{aligned} \sum_{t_j \in \Omega_{\infty}^2} \|\mathbf{X}_{t_j+1} - \mathbf{X}_{t_j}\|_F^2 &\leq \frac{a_2}{c_1}, \\ \sum_{t_j \in \Omega_{\infty}^2} \|\mathbf{S}_{t_j+1} - \mathbf{S}_{t_j}\|_F^2 &\leq \frac{2a_2}{\tau - \rho}. \end{aligned}$$

Again from Assumption A2, we have

$$\lim_{\|\mathbf{X}\|_F \rightarrow \infty \text{ or } \|\mathbf{S}\|_F \rightarrow \infty} f(\mathbf{X}, \mathbf{S}) \rightarrow \infty. \quad (51)$$

Thus, $\max_{t_j=1,\dots,\infty} \|[\mathbf{X}_{t_j}, \mathbf{S}_{t_j}]\|_F < \infty$, and the sequence $\{[\mathbf{X}_{t_j}, \mathbf{S}_{t_j}]\}$ is bounded with at least one limit point [51].

- 2) $|\Omega_\infty^1|$ is infinite but $|\Omega_\infty^2|$ is finite: For $t_j \in \Omega_\infty^1$, from (47) and (48), we have $F(\mathbf{X}_{t_j+1}, \mathbf{S}_{t_j+1}) \leq F(\mathbf{X}_{t_j}, \mathbf{S}_{t_j})$. As, F is bounded from below (Assumption A2), the sequence $\{F([\mathbf{X}_{t_j}, \mathbf{S}_{t_j}])\}$ must be bounded. Besides, again from Assumption A2, we have (51), which indicates the sequence $[\mathbf{X}_{t_j}, \mathbf{S}_{t_j}]$ must be bounded with at least one limit point [51].
- 3) Both $|\Omega_\infty^1|$ and $|\Omega_\infty^2|$ are infinite: As in the above two cases, $\{[\mathbf{X}_t, \mathbf{S}_t]\}$ is bounded with at least one limit point once $|\Omega_\infty^1|$ or $|\Omega_\infty^2|$ is infinite.

Thus, the sequence $\{[\mathbf{X}_t, \mathbf{S}_t]\}$ generated from Algorithm 6 is bounded and has at least one limit point. \square

C.13 Corollary 4.2

Proof. Let $c_2 = \min(\delta/2, c_1)$. First, we have

$$\begin{aligned} & \sum_{t \in \Omega_T^1} \frac{\delta}{2} (\|\mathbf{X}_{t+1} - \mathbf{Y}_t^{\mathbf{X}}\|_F^2 + \|\mathbf{S}_{t+1} - \mathbf{Y}_t^{\mathbf{S}}\|_F^2) \\ & + \sum_{t \in \Omega_T^2} (c_1 \|\mathbf{X}_{t+1} - \mathbf{X}_t\|_F^2 + \frac{\tau - \rho}{2} \|\mathbf{S}_{t+1} - \mathbf{S}_t\|_F^2) \\ & \geq c_2 \sum_{t=1}^T \|[\mathbf{X}_{t+1}, \mathbf{S}_{t+1}] - \mathbf{C}_t\|_F^2. \end{aligned} \quad (52)$$

Together with (49) and (50), we have

$$\begin{aligned} & \min_{t=1,\dots,T} \|[\mathbf{X}_{t+1}, \mathbf{S}_{t+1}] - \mathbf{C}_t\|_F^2 \\ & \leq \frac{1}{T} \sum_{t=1}^T \|[\mathbf{X}_{t+1}, \mathbf{S}_{t+1}] - \mathbf{C}_t\|_F^2 \\ & \leq \sum_{t=1}^{\infty} \|[\mathbf{X}_{t+1}, \mathbf{S}_{t+1}] - \mathbf{C}_t\|_F^2 \\ & \leq \frac{F(\mathbf{X}_1, \mathbf{S}_1) - \inf F}{c_2 T}, \end{aligned}$$

where the last inequality comes from (52). \square

C.14 Theorem 4.3

Proof. Let $g = \check{g} + \tilde{g}$ be the difference of convex decomposition of g . As two blocks of variables are involved, its critical points are defined as follows.

Definition 3 ([39]). If \mathbf{X} and \mathbf{S} satisfy

$$\begin{aligned} \mathbf{0} & \in \nabla_{\mathbf{X}} f(\mathbf{X}, \mathbf{S}) + \lambda (\partial \check{r}(\mathbf{X}) - \partial \tilde{r}(\mathbf{X})), \\ \mathbf{0} & \in \nabla_{\mathbf{S}} f(\mathbf{X}, \mathbf{S}) + \lambda (\partial \check{g}(\mathbf{S}) - \partial \tilde{g}(\mathbf{S})), \end{aligned}$$

then $[\mathbf{X}, \mathbf{S}]$ is a critical point of F .

Lemma C.8 ([37]). If \mathbf{X} and \mathbf{S} satisfy

$$\begin{aligned} \mathbf{X} & = \text{prox}_{\frac{\lambda}{\tau}}(\mathbf{X} - \frac{1}{\tau} \nabla_{\mathbf{X}} f(\mathbf{X}, \mathbf{S})), \\ \mathbf{S} & = \text{prox}_{\frac{\nu}{\tau}}(\mathbf{S} - \frac{1}{\tau} \nabla_{\mathbf{S}} f(\mathbf{X}, \mathbf{S})), \end{aligned}$$

then $[\mathbf{X}, \mathbf{S}]$ is a critical point of F .

Partition $\{1, \dots, \infty\}$ into two sets as Ω_∞^1 and Ω_∞^2 , where $t \in \Omega_\infty^1$ if steps 10-11 are performed; otherwise, $t \in \Omega_\infty^2$ (and steps 13-14 are performed), we consider three cases here.

- 1) $|\Omega_\infty^1|$ is finite but $|\Omega_\infty^2|$ is infinite: Let $\{[\mathbf{X}_{t_j}, \mathbf{S}_{t_j}]\}$ be a subsequence of $\{[\mathbf{X}_t, \mathbf{S}_t]\}$ where $t \in \Omega_\infty^2$, and

$$\lim_{t_j \rightarrow \infty} [\mathbf{X}_{t_j}, \mathbf{S}_{t_j}] = [\mathbf{X}_*, \mathbf{S}_*].$$

From (49), we have

$$\begin{aligned} & \sum_{t=1}^{\infty} \|\mathbf{X}_{t+1} - \mathbf{X}_t\|_F^2 < \infty, \\ & \sum_{t=1}^{\infty} \|\mathbf{S}_{t+1} - \mathbf{S}_t\|_F^2 < \infty. \end{aligned}$$

These indicate

$$\lim_{t_j \rightarrow \infty} \mathbf{X}_{t_j+1} - \mathbf{X}_{t_j} = \mathbf{0}, \quad (53)$$

$$\lim_{t_j \rightarrow \infty} \mathbf{S}_{t_j+1} - \mathbf{S}_{t_j} = \mathbf{0}. \quad (54)$$

From (53), we have

$$\lim_{t_j \rightarrow \infty} \mathbf{X}_{t_j+1} = \lim_{t_j \rightarrow \infty} \mathbf{X}_{t_j} = \mathbf{X}_*. \quad (55)$$

Combining (53) and (55), we have

$$\begin{aligned} \lim_{t_j \rightarrow \infty} \mathbf{X}_{t_j+1} & = \text{InexactPS} \left(\lim_{t_j \rightarrow \infty} \mathbf{X}_{t_j}, \lim_{t_j \rightarrow \infty} \mathbf{R}_{t_j} \right) \\ & = \text{InexactPS} \left(\mathbf{X}_*, \lim_{t_j \rightarrow \infty} \mathbf{R}_{t_j} \right) \\ & = \mathbf{X}_*. \end{aligned}$$

Thus,

$$\mathbf{X}_* = \text{prox}_{\frac{\lambda}{\tau}}(\mathbf{X}_* - \frac{1}{\tau} \nabla_{\mathbf{X}} f(\mathbf{X}_*, \mathbf{S}_*)) \quad (56)$$

holds by the assumption. Then, the proximal operator is always exact for \mathbf{S} . Using (54), we have

$$\begin{aligned} \lim_{t_j \rightarrow \infty} \mathbf{S}_{t_j+1} & = \lim_{t_j \rightarrow \infty} \text{prox}_{\frac{\nu}{\tau}}(\mathbf{S}_{t_j} - \frac{1}{\tau} \nabla_{\mathbf{S}} f(\mathbf{X}_{t_j}, \mathbf{S}_{t_j})) \\ & = \text{prox}_{\frac{\nu}{\tau}}(\mathbf{S}_* - \frac{1}{\tau} \nabla_{\mathbf{S}} f(\mathbf{X}_*, \mathbf{S}_*)) \\ & = \mathbf{S}_* \end{aligned} \quad (57)$$

Combining with (56) and (57), $[\mathbf{X}_*, \mathbf{S}_*]$ is a critical point of (11) by using Lemma C.8.

- 2) $|\Omega_\infty^1|$ is infinite but $|\Omega_\infty^2|$ is finite: Let $\{[\mathbf{X}_{t_j}, \mathbf{S}_{t_j}]\}$ be a subsequence of $\{[\mathbf{X}_t, \mathbf{S}_t]\}$ where $t \in \Omega_\infty^1$, and

$$\lim_{t_j \rightarrow \infty} [\mathbf{X}_{t_j}, \mathbf{S}_{t_j}] = [\mathbf{X}_*, \mathbf{S}_*].$$

From (49), we have

$$\begin{aligned} & \sum_{t_j \in \Omega_\infty^2} \|\mathbf{X}_{t_j+1} - \mathbf{Y}_{t_j}^{\mathbf{X}}\|_F^2 \leq \infty, \\ & \sum_{t_j \in \Omega_\infty^2} \|\mathbf{S}_{t_j+1} - \mathbf{Y}_{t_j}^{\mathbf{S}}\|_F^2 \leq \infty, \end{aligned}$$

and then

$$\lim_{t_j \rightarrow \infty} \mathbf{X}_{t_j+1} - \mathbf{Y}_{t_j}^{\mathbf{X}} = \mathbf{0}, \quad (58)$$

$$\lim_{t_j \rightarrow \infty} \mathbf{S}_{t_j+1} - \mathbf{Y}_{t_j}^{\mathbf{S}} = \mathbf{0}. \quad (59)$$

Thus,

$$\lim_{t_j \rightarrow \infty} \mathbf{X}_{t_j+1} = \lim_{t_j \rightarrow \infty} \mathbf{Y}_{t_j}^{\mathbf{X}} = \mathbf{X}_*. \quad (60)$$

Combing (58) and (60), we have

$$\begin{aligned} \lim_{t_j \rightarrow \infty} \mathbf{X}_{t_j+1} &= \text{InexactPS} \left(\lim_{t_j \rightarrow \infty} \mathbf{Y}_{t_j}^{\mathbf{X}}, \lim_{t_j \rightarrow \infty} \mathbf{R}_{t_j} \right) \\ &= \text{InexactPS} \left(\mathbf{X}_*, \lim_{t_j \rightarrow \infty} \mathbf{R}_{t_j} \right) \\ &= \mathbf{X}_*. \end{aligned}$$

Thus,

$$\mathbf{X}_* = \text{prox}_{\frac{\lambda}{\tau}}(\mathbf{X}_* - \frac{1}{\tau} \nabla_{\mathbf{X}} f(\mathbf{X}_*, \mathbf{S}_*)) \quad (61)$$

holds by the assumption. Then, the proximal operator is always exact for \mathbf{S} . Using (59),

$$\begin{aligned} \lim_{t_j \rightarrow \infty} \mathbf{S}_{t_j+1} &= \lim_{t_j \rightarrow \infty} \text{prox}_{\frac{\mu}{\tau}}(\mathbf{Y}_{t_j}^{\mathbf{S}} - \frac{1}{\tau} \nabla_{\mathbf{S}} f(\mathbf{Y}_{t_j}^{\mathbf{X}}, \mathbf{Y}_{t_j}^{\mathbf{S}})) \\ &= \text{prox}_{\frac{\mu}{\tau}}(\mathbf{S}_* - \frac{1}{\tau} \nabla_{\mathbf{S}} f(\mathbf{X}_*, \mathbf{S}_*)) \\ &= \mathbf{S}_* \end{aligned} \quad (62)$$

Combining with (61) and (62), $[\mathbf{X}_*, \mathbf{S}_*]$ is a critical point of (11) by using Lemma C.8.

- 3) Both $|\Omega_{\infty}^1|$ and $|\Omega_{\infty}^2|$ are infinite: As above, either $|\Omega_{\infty}^1|$ or $|\Omega_{\infty}^2|$ is infinite, a limit point $[\mathbf{X}_*, \mathbf{S}_*]$ is a critical point of (11).

Thus, the limit points of the sequence $\{[\mathbf{X}_t, \mathbf{S}_t]\}$ are also critical points of (11). \square

C.15 Proposition 5.1

Proof. As the SVD of $\mathbf{A}^{\top} \mathbf{A}$ is $\mathbf{V} \mathbf{\Sigma} \mathbf{V}^{\top}$, the SVD of \mathbf{A} can be written as $\mathbf{U} \mathbf{\Sigma}^{\frac{1}{2}} \mathbf{V}^{\top}$ where \mathbf{U} is an orthogonal matrix containing the span of \mathbf{A} . From the construction of \mathbf{w} , we have

$$\begin{aligned} \mathbf{A} \mathbf{V} (\text{Diag}(\mathbf{w}))^{-\frac{1}{2}} &= \mathbf{U} \mathbf{\Sigma}^{\frac{1}{2}} (\mathbf{V}^{\top} \mathbf{V}) (\text{Diag}(\mathbf{w}))^{-\frac{1}{2}} \\ &= \mathbf{U} \mathbf{\Sigma}^{\frac{1}{2}} (\text{Diag}(\mathbf{w}))^{-\frac{1}{2}}. \end{aligned}$$

Consider the two cases.

- 1) \mathbf{A} is of full column rank: Then,

$$\mathbf{U} \mathbf{\Sigma}^{\frac{1}{2}} (\text{Diag}(\mathbf{w}))^{-\frac{1}{2}} = \mathbf{U} \left(\mathbf{\Sigma}^{\frac{1}{2}} \mathbf{\Sigma}^{-\frac{1}{2}} \right) = \mathbf{U},$$

which contains the span of \mathbf{A} .

- 2) Assume that \mathbf{A} has k columns and its rank is $\bar{k} < k$: Then,

$$\begin{aligned} &\mathbf{U} \mathbf{\Sigma}^{\frac{1}{2}} (\text{Diag}(\mathbf{w}))^{-\frac{1}{2}} \\ &= \mathbf{U} \text{Diag} \left(\Sigma_{11}^{\frac{1}{2}}, \dots, \Sigma_{\bar{k}\bar{k}}^{\frac{1}{2}}, 0, \dots, 0 \right) \\ &\quad \text{Diag} \left(\Sigma_{11}^{-\frac{1}{2}}, \dots, \Sigma_{\bar{k}\bar{k}}^{-\frac{1}{2}}, 1, \dots, 1 \right) \\ &= [\mathbf{U}_{\bar{k}}, \mathbf{0}], \end{aligned}$$

where $\mathbf{U}_{\bar{k}}$ contains the first \bar{k} columns of \mathbf{U} . As \mathbf{A} is only of rank \bar{k} , $\mathbf{U} \mathbf{\Sigma}^{\frac{1}{2}} (\text{Diag}(\mathbf{w}))^{-\frac{1}{2}}$ again covers the span of \mathbf{A} .

The Proposition then follows. \square

C.16 Proposition 5.2

Proof. Let the SVD of \mathbf{B} be $\bar{\mathbf{U}} \bar{\mathbf{\Sigma}} \bar{\mathbf{V}}^{\top}$. Then,

$$\mathbf{P}^{\top} \mathbf{B} = (\mathbf{P}^{\top} \bar{\mathbf{U}}) \bar{\mathbf{\Sigma}} \bar{\mathbf{V}}^{\top}.$$

Note that

$$\begin{aligned} (\mathbf{P}^{\top} \bar{\mathbf{U}})^{\top} \mathbf{P}^{\top} \bar{\mathbf{U}} &= \bar{\mathbf{U}}^{\top} (\mathbf{P} \mathbf{P}^{\top}) \bar{\mathbf{U}} \\ &= \bar{\mathbf{U}}^{\top} (\bar{\mathbf{U}} \bar{\mathbf{U}}^{\top}) \bar{\mathbf{U}} = \mathbf{I}, \end{aligned}$$

where the second equality comes from

$$\text{span}(\mathbf{P}) = \text{span}(\bar{\mathbf{U}}). \quad (63)$$

Thus, the SVD of $\mathbf{P}^{\top} \mathbf{B}$ is $(\mathbf{P}^{\top} \bar{\mathbf{U}}) \bar{\mathbf{\Sigma}} \bar{\mathbf{V}}^{\top}$. As a result, we have $\mathbf{V} = \bar{\mathbf{V}}$, $\mathbf{\Sigma} = \bar{\mathbf{\Sigma}}$. Finally, from $\mathbf{U} = \mathbf{P}^{\top} \bar{\mathbf{U}}$, we have

$$\mathbf{P} \mathbf{U} = \mathbf{P} \mathbf{P}^{\top} \bar{\mathbf{U}} = \bar{\mathbf{U}} (\bar{\mathbf{U}}^{\top} \bar{\mathbf{U}}) = \bar{\mathbf{U}},$$

where the second equality again comes from (63). \square